

A Model of a CA3 Hippocampal Pyramidal Neuron Incorporating Voltage-Clamp Data on Intrinsic Conductances

ROGER D. TRAUB, ROBERT K. S. WONG, RICHARD MILES, AND HILLARY MICHELSON

IBM Research Division, IBM T. J. Watson Research Center, Yorktown Heights 10598; Department of Neurology, Columbia University, New York 10032; Department of Pharmacology, State University of New York, Brooklyn, New York, 11203; and Laboratoire de Neurobiologie Cellulaire, Institut Pasteur, 75724 Paris Cedex 15, France

SUMMARY AND CONCLUSIONS

1. We have developed a 19-compartment cable model of a guinea pig CA3 pyramidal neuron. Each compartment is allowed to contain six active ionic conductances: g_{Na} , g_{Ca} , $g_{K(DR)}$ (where DR stands for delayed rectifier), $g_{K(A)}$, $g_{K(AHP)}$, and $g_{K(C)}$. The conductance g_{Ca} is of the high-voltage activated type. The model kinetics for the first five of these conductances incorporate voltage-clamp data obtained from isolated hippocampal pyramidal neurons. The kinetics of $g_{K(C)}$ are based on data from bullfrog sympathetic neurons. The time constant for decay of submembrane calcium derives from optical imaging of Ca signals in Purkinje cell dendrites.

2. To construct the model from available voltage-clamp data, we first reproduced current-clamp records from a model isolated neuron (soma plus proximal dendrites). We next assumed that ionic channel kinetics in the dendrites were the same as in the soma. In accord with dendritic recordings and calcium-imaging data, we also assumed that significant g_{Ca} occurs in dendrites. We then attached sections of basilar and apical dendritic cable. By trial and error, we found a distribution (not necessarily unique) of ionic conductance densities that was consistent with current-clamp records from the soma and dendrites of whole neurons and from isolated apical dendrites.

3. The resulting model reproduces the Ca^{2+} -dependent spike depolarizing afterpotential (DAP) recorded after a stimulus subthreshold for burst elicitation.

4. The model also reproduces the behavior of CA3 pyramidal neurons injected with increasing somatic depolarizing currents: low-frequency (0.3–1.0 Hz) rhythmic bursting for small currents, with burst frequency increasing with current magnitude; then more irregular bursts followed by afterhyperpolarizations (AHPs) interspersed with brief bursts without AHPs; and finally, rhythmic action potentials without bursts.

5. The model predicts the existence of still another firing pattern during tonic depolarizing dendritic stimulation: brief bursts at <1 to ~12 Hz, a pattern not observed during somatic stimulation. These bursts correspond to rhythmic dendritic calcium spikes.

6. The model CA3 pyramidal neuron can be made to resemble functionally a CA1 pyramidal neuron by increasing $\bar{g}_{K(DR)}$ and decreasing dendritic \bar{g}_{Ca} and $\bar{g}_{K(C)}$. Specifically, after these alterations, tonic depolarization of the soma leads to adapting repetitive firing, whereas stimulation of the distal dendrites leads to bursting.

7. A critical set of parameters concerns the regulation of the pool of intracellular $[Ca^{2+}]$ that interacts with membrane channels ($g_{K(C)}$ and $g_{K(AHP)}$), particularly in the dendrites. For dendritic calcium spikes to occur at ~12 Hz, it appears necessary to postulate a time constant of <20 ms for decay of the intracellular $[Ca^{2+}]$ in this pool.

8. This revised cellular model has been incorporated into a network of neurons with mutual excitation via both quisqualate and *N*-methyl-D-aspartate receptor types. Such a model network is able to reproduce picrotoxin-induced synchronized multiple bursts. Repetitive dendritic calcium spikes appear to be crucial for the phenomenon of multiple bursts.

INTRODUCTION

Modeling the electrotonic and active properties of neurons is a useful exercise. It helps one to understand how synaptic inputs impinging on different membrane regions are integrated to produce an output signal. Models of neurons are also useful as building blocks for the construction of network models. A network model helps one to understand how intrinsic cellular properties combine with the properties of connections between neurons to generate meaningful population behaviors. Modeling of hippocampal pyramidal neurons, in particular, is helpful because these cells contain active dendritic currents that can generate high-frequency bursts of action potentials, giving rise to complex integrational characteristics (Masukawa and Prince 1984; Wong et al. 1979). At the population level, groups of hippocampal neurons generate a variety of interesting behaviors, including synchronized epileptiform bursts (Schwartzkroin and Prince 1977) and low-amplitude oscillations (Schneiderman 1986; Schwartzkroin and Haglund 1986). Such behaviors can be seen in vitro in groups of only a few thousand cells, offering the hope of a detailed analysis.

We have already twice attempted to model the electrical properties of a hippocampal pyramidal cell. In the first attempt, partly in analogy with Purkinje cells, a calcium conductance was located exclusively in the dendrites, whereas a sodium- and voltage-dependent K conductance were located in the somatic region and in isolated dendritic "hot spots" (Traub and Llinás 1979). Because intradendritic recordings suggested that bursting (with sodium- and calcium-dependent action potentials) could be independently produced in both soma and dendrites, a second model was constructed using a different approach (Traub 1982). Distinct membrane regions were assumed to contain all of the requisite conductances to generate a burst and its associated long afterhyperpolarization (AHP) (Hotson and Prince 1980). Four active conductances were used in each active membrane region— g_{Na} , g_{Ca} , g_K , and $g_{K(Ca)}$ —and the kinetics were inferred from current-clamp records. To pro-

duce bursts in a localized membrane region, it was necessary to postulate 1) a rapid inactivation (tens of milliseconds) of g_{Ca} by intracellular $[Ca^{2+}]$, an assumption that now seems unlikely (A. Kay, personal communication); and 2) a voltage-dependent inactivation of g_K . The bursts produced by this model appeared realistic, and the frequency of bursting increased appropriately with progressive depolarization. The model did not, however, switch from repetitive bursting to repetitive single-action potentials with further depolarization, in contrast to CA3 pyramidal cells recorded *in vitro* (Wong and Prince 1981).

The model pyramidal cell was nevertheless useful as a building block in network models. Network models were able to reproduce synchronized bursts in disinhibited slices (Traub and Wong 1982), the varying effects one cell exerts on another in the network as inhibition is reduced (Traub et al. 1987), and spontaneous population oscillations that occur in partially disinhibited slices (Miles and Wong 1987a; Schneiderman 1986; Schwartzkroin and Haglund 1986; Traub et al. 1989), to name a few (Traub and Miles, 1991b). These network simulations also made some predictions that were subsequently verified, including 1) the ability of a burst in one CA3 cell to evoke a burst in a postsynaptic pyramidal cell (Miles and Wong 1986) and 2) the ability of a single cell to synchronize the entire population (Miles and Wong 1983). Nevertheless, the model had certain inadequacies. In addition to its inability to switch to a repetitive firing mode when sufficiently depolarized, the 1982 model when incorporated into networks would not generate the synchronized multiple bursts that are observed when slices are bathed in the γ -aminobutyric acid-A (GABA_A) blocker picrotoxin (Hablitz 1984; Miles et al. 1984) unless axonal conduction block with rapid recovery was postulated (Traub et al. 1984). Possibly this failure could be related to the inability of the model neuron to generate dendritic calcium spikes at the requisite frequency (roughly 10–15 Hz).

We therefore wondered whether a more accurate cellular model would help to understand these (and other) scientific issues: why and how pyramidal neurons can switch between different firing modes and what neuronal properties might be critical for the generation of synchronized multiple bursts in a population of cells.

Two additional types of data have become available and prompted us to attempt yet another pyramidal cell model. Whole-cell recording of membrane currents from the isolated cell preparation (Kay and Wong 1986) has permitted a more precise characterization of many of the voltage-dependent currents in these neurons. Furthermore, calcium-imaging studies suggest that g_{Ca} is widely spread over the cell membrane (Regehr et al. 1989). Our approach has been to use the voltage-clamp data to define or at least constrain the current kinetics and then to search for a distribution of conductance densities over the cell membrane that was consistent with current-clamp records from both soma and dendrites. The resulting model has certain features of both previous models. As in the 1979 version, the single type of g_{Ca} used is predominantly dendritic and g_{Na} is relatively localized to particular membrane regions; in addition, as in the 1982 version, localized parts of the cell can produce bursts, although the burst morphology depends on the region of the cell. The new model exhibits either repetitive

bursting or repetitive single action potentials as a function of membrane potential in a realistic way. Both CA3 and CA1 types of firing behavior can be reproduced by proper manipulation of the membrane conductance densities. In addition, networks of the new model neurons, with mutual excitation mediated by quisqualate (QUIS) and *N*-methyl-D-aspartate (NMDA) types of synaptic actions, are also able to generate synchronized multiple bursts. Two well-defined experimental predictions are suggested by the new model, one at the level of individual cells and the other at the population level. A large number of simulations suggest that network behaviors that were exhibited by the 1982 model, such as synchronized population oscillations, are still reproduced using the new model as a cellular building block.

We wish to emphasize that, despite the wealth of data on membrane properties of hippocampal neurons, the data are not sufficient to define all the parameters that one would like. Furthermore, some of the data from different laboratories appear to be mutually contradictory. We have attempted to construct a model consistent with as many data as we could, but our model is not unique (in terms of the membrane distribution of conductance densities, for example), nor does it reproduce every known feature of the behavior of these cells. In addition to describing the construction and properties of the cell model, we shall try (in METHODS) to give some feel for how the behavior depends on certain parameter choices.

Some of these data have been presented in abstract form (Traub et al. 1990).

Glossary

C_k	capacitance of compartment k ($k = 1, \dots, 19$) (nF)
$g_{L,k}$	leakage conductance for compartment k (μS)
$\gamma_{k,l}$	conductance between compartments k and l ($= 0$, unless $k = l \pm 1$)
$\bar{g}_{Na,k}$	maximum conductance for sodium in compartment k (μS)
$\bar{g}_{Ca,k}$	maximum conductance for calcium in compartment k (μS). g_{Ca} is high-voltage activated, slowly inactivating
$\bar{g}_{K(DR),k}$	maximum conductance for delayed rectifier K current in compartment k (μS)
$\bar{g}_{K(A),k}$	maximum conductance for A-type of transient K current in compartment k (μS)
$\bar{g}_{K(AHP),k}$	maximum conductance for long-duration Ca-dependent AHP K current in compartment k (μS)
$\bar{g}_{K(C),k}$	maximum conductance for short-duration voltage- and Ca-dependent K current in compartment k (μS)
m_k	activation variable for sodium current in compartment k (dimensionless)
h_k	inactivation variable for sodium current in compartment k (dimensionless)
s_k	activation variable for calcium current in compartment k (dimensionless)
r_k	inactivation variable for calcium current in compartment k (dimensionless)
n_k	activation variable for delayed rectifier K current in compartment k (dimensionless)
a_k	activation variable for transient K current in compartment k (dimensionless)
b_k	inactivation variable for transient K current in compartment k (dimensionless)
g_k	activation variable for AHP K current in compartment k (dimensionless)

c_k	activation variable for voltage- and calcium-dependent K current in compartment k (dimensionless)
$I_{\text{Ca},k}$	calcium current of compartment k (nA)
$I_{\text{ionic},k}$	transmembrane ionic current of compartment k (understood to be at time t , but time dependence not written explicitly) (nA)
$I_{\text{synaptic},k}$	total synaptic current for compartment k (nA)
t	time (ms)
V_k	transmembrane potential of compartment, relative to rest, mV
$V_{\text{Na}}, V_{\text{Ca}}, V_K$	reversal potentials, relative to resting potential, for Na^+ , Ca^{2+} , and K^+ ions, respectively. Values are 115, 140, and -15 mV, respectively. These are held constant (i.e., V_{Ca} does not depend on x)
χ_k	Ca^{2+} concentration in shell beneath membrane of compartment k . For the present model, the units are arbitrary (because the depth of the appropriate shell is unknown)
β_x	Inverse time constant for (1st-order) relaxation of the χ_k . Assumed to be the same for all compartments. Value is 0.075 ms^{-1} , corresponding to a time constant of 13.33 ms
ϕ_k	scaling constant for compartment k to convert Ca current to Ca concentration in a shell beneath membrane; may be different for different compartments, depending on dimensions of shell. Units arbitrary. Values used were $\phi_1 = 7,769$ ($i = 1, \dots, 7$); $\phi_8 = 34,530$; $\phi_9 = 17,402$, $\phi_{10} = 26,404$; $\phi_i = 5,941$. The different values result from different dendritic membrane areas, as well as different shell thickness for the soma and adjacent membrane (compartments 8–10) compared with remainder of the dendrites. The larger ϕ for the soma and adjacent membrane means that a given I_{Ca} leads to a larger and faster calcium transient in the corresponding shell

METHODS

Acutely isolated cells

CA3 pyramidal neurons were isolated from adult guinea pigs (weight 200–400g) and whole-cell recordings were obtained by the use of methods described by Kay and Wong (1986) and Numann et al. (1987).

Structure of model and electrotonic parameters

The structure of the compartmental model is illustrated at the bottom of Fig. 1. It is the same structure as before (Traub 1982) except that dendritic branching is omitted. The basilar (*left*) and apical (*right*) dendrites are each represented by an equivalent cylinder (Rall 1962a). This is a reasonable description in view of the approximate $\frac{1}{2}$ power branching of hippocampal pyramidal cell dendrites (Turner and Schwartzkroin 1980). As before, we do not consider the nonuniform electrotonic length of different dendrites. Each dendritic compartment represents 0.1λ of membrane, and there are 19 compartments in all (8 for the basilar dendrites, 1 for the soma, and 10 for the apical dendrites). The parameters that define the structure and electrotonic properties of the model are as follows: $R_i = 100 \Omega\text{-cm}$, $R_m = 10,000 \Omega\text{-cm}^2$, $C_m = 3 \mu\text{F}/\text{cm}^2$ (Turner and Schwartzkroin 1980), $\tau_M = 30 \text{ ms}$, input resistance apical dendrite = $60 \text{ M}\Omega$, input resistance basilar dendrite = $90 \text{ M}\Omega$, and input resistance of the whole cell = $32 \text{ M}\Omega$. The whole-cell input resistance is in the observed range (at least as recorded with sharp electrodes); Turner and Schwartzkroin (1983) obtained an average input resistance of $33 \text{ M}\Omega$ for CA3 pyramidal cells. Horseradish peroxidase injections of CA3 cells combined with electrical measurements led to an estimate of $\sim 67 \text{ M}\Omega$ for the

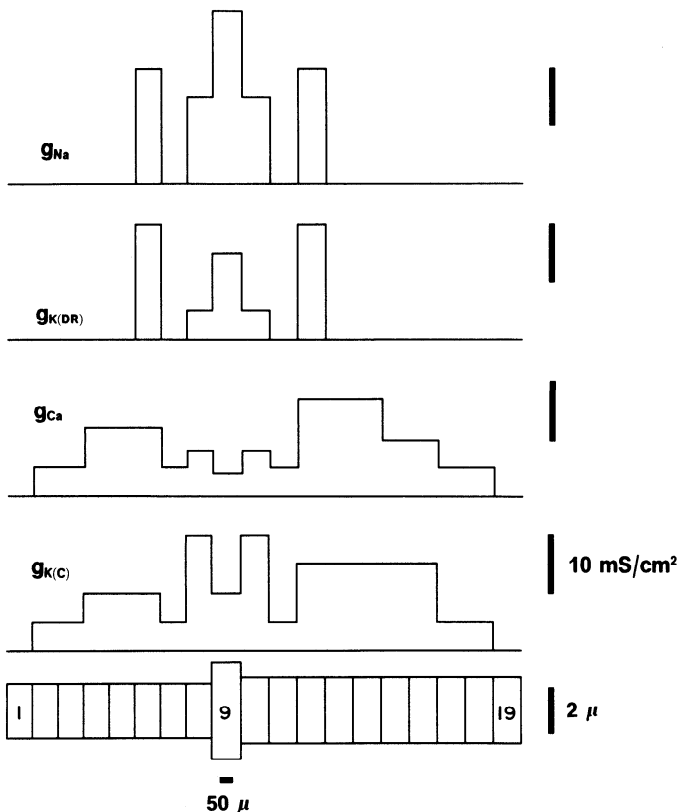


FIG. 1. Densities of 4 of the ionic conductances in the CA3 pyramidal cell model. Electrotonic structure of the model is shown below; note the different horizontal and vertical scales. Basilar dendrites are to the left and apical dendrites to the right. Conductance density is drawn over each compartment according to the scale on the right. Numbers of certain compartments are indicated in the bottom part.

average input resistance of the apical dendrites and $94 \text{ M}\Omega$ for the basilar dendrites (D. A. Turner, personal communication).

The soma dimensions were radius $4.23 \mu\text{m}$, length $125 \mu\text{m}$, area $3,320 \mu\text{m}^2$. Although the shape of the soma is not realistic (it is too long and narrow), its area is reasonable. For example, if the soma were approximated by a cone of basal radius $12.5 \mu\text{m}$ (r) and height $75 \mu\text{m}$ (h), the area would be $\pi r\sqrt{r^2 + h^2} + \pi r^2 = 3,477 \mu\text{m}^2$.

The dimensions of an apical compartment were radius $2.89 \mu\text{m}$, length $120 \mu\text{m}$ (hence $1\lambda = 1,200 \mu\text{m} = 0.12 \text{ cm}$), area $2,188 \mu\text{m}^2$. Because λ in cm = $\sqrt{rR_m/2R_i} = \sqrt{(0.000289 \times 10,000)/200} = 0.120 \text{ cm}$, these numbers are consistent with each other.

The dimensions of a basilar compartment were radius $2.42 \mu\text{m}$, length $110 \mu\text{m}$, area = $1,673 \mu\text{m}^2$. The reader should recall that the equivalent cylinder corresponding to a branching dendrite is longer than the original dendrite (Rall 1962b), so that distances along the equivalent cylinder do not directly match distances alongside the actual neuron. A coordinate transformation must be applied for the match.

Simulations were run not only in the entire structure shown in Fig. 1, but also in pieces of it. We simulated an acutely isolated neuron as a soma with an adjacent basilar and apical dendritic compartment. Isolated apical and dendritic cables were simulated, as were neurons with the apical and/or basilar cylinders truncated. In all such cases, the ends of the dendritic cylinders were sealed. We did not correct for the apparent increase in membrane resistivity that occurs in isolated cells (Kay and Wong 1986; Storm 1990).

Physics of the model

Voltage excursions in a cable model, in general, are described by the cable equation (Rall 1989). For a compartmental model, we of

course use a version of the cable equation that is discrete in space and continuous in time. First, let us outline our system of units and our notation. We use a consistent set of units: mV, nA, ms, nF, and μ S. Membrane potentials are written relative to resting potential. The extracellular space is assumed to be isopotential. In our notation, the second subscript (k or i) is used to index the compartment number (Fig. 1, bottom). The letter C is used for a capacitance. Subscript L refers to the leakage conductance or current; and Na, Ca, and K refer to the respective ions. V_{Na} , V_{Ca} , and V_{K} are constants that represent the respective equilibrium potentials. The bar superscript, as in \bar{g}_{Ca} , denotes the maximum ionic conductance of a particular type in a particular compartment; the actual conductance at a given time will be the product of the (constant) \bar{g} term with appropriate voltage- and/or calcium-dependent dimensionless variables. The subscripts K(DR), K(A), K(AHP), and K(C) refer to the four types of K currents in the model: DR stands for delayed rectifier, A for the A-type of transient current, AHP for the long-duration Ca-dependent AHP current (Hotson and Prince 1980; Lancaster and Adams 1986; Lancaster and Nicoll 1987; Numann et al. 1987), and C for the short-duration Ca- and voltage-dependent current (Adams et al. 1982; Alger and Williamson 1988; Lancaster and Nicoll 1987). The letters m , h , s , r , n , a , b , q , and c denote dimensionless membrane-state variables that control the various ionic conductances; their values lie between 0 and 1. χ is the calcium concentration in a "shell" beneath the membrane. This shell can be considered as a cytoplasmic compartment attached to the inside of each membrane compartment. χ grows by transmembrane influx of Ca (intracellular Ca release not being considered) and declines by first-order decay with time constant β_{χ}^{-1} . χ in turn regulates the local AHP and C conductances. Radial and axial diffusion of calcium are not simulated in the model, nor are cytoplasmic uptake and buffering of calcium explicitly simulated. Many of these terms are recapitulated in the equations below and in the *Glossary* (see INTRODUCTION).

The spatially discrete form of the cable equation can then be written

$$C_k \frac{dV_k}{dt} = \gamma_{k-1,k}(V_{k-1} - V_k) + \gamma_{k+1,k}(V_{k+1} - V_k) - I_{\text{ionic},k} \quad (1)$$

The ionic current to compartment k is a sum of the leakage current (with leakage conductance assumed to be independent of membrane potential), possibly synaptic currents, various voltage-dependent "active" currents, and perhaps an injected current

$$\begin{aligned} I_{\text{ionic},k} = & g_{L,k}V_k + I_{\text{synaptic},k} + \bar{g}_{\text{Na}}m_k^2h_k(V_k - V_{\text{Na}}) + \bar{g}_{\text{Ca}}s_k^2r_k(V_k - V_{\text{Ca}}) \\ & + \bar{g}_{\text{K(}(\text{DR})\text{)}}n(V_k - V_{\text{K}}) + \bar{g}_{\text{K(A)}}ab(V_k - V_{\text{K}}) + \bar{g}_{\text{K(AHP)}}q(V_k - V_{\text{K}}) \\ & + \bar{g}_{\text{K(C)}}c \times \min\left(1, \frac{\chi_k}{250}\right) \times (V_k - V_{\text{K}}) - I_{\text{injected},k} \quad (2) \end{aligned}$$

The above equation describes the relation of specific membrane-state variables and submembrane Ca to ionic conductances.

The synaptic currents that we shall consider in this paper are excitatory only and occur onto two compartments: numbers 3 and 15, each 0.6λ from the soma in the basilar or apical direction, respectively (the compartment numbering is indicated in Fig. 1). A presynaptic action potential induces a fast excitatory postsynaptic potential (EPSP) in compartments 3 and 15 (corresponding to QUIS receptor activation) and a slow voltage-dependent EPSP in compartment 15 (corresponding to NMDA receptor activation). The QUIS synaptic current in each compartment is $c_{\text{QUIS}}e^{-t/2} \times (V - 60)$, where V is the local membrane potential and 60 mV is the EPSP reversal potential relative to rest. The 2-ms time constant is consistent with the voltage-clamp data of Brown and Johnston (1983) on the mossy fiber EPSP; this QUIS component may correspond to the rapidly inactivating quisqualate-activated con-

ductance reported by Tang et al. (1989) in cultured hippocampal neurons. The NMDA EPSP is more complicated (Nowak et al. 1984). A presynaptic action potential induces a ligand-gated "virtual conductance," $g(t)$, which peaks at 2 ms in the model and decays with time constant of 100–150 ms (Forsythe and Westbrook 1988). Both the onset and decay kinetics that we used may be, if anything, too rapid (Lester et al. 1990). The actual synaptic conductance is the virtual conductance (ligand-dependent) times a voltage- and magnesium-dependent Boltzmann term. The form of the Boltzmann term that we use is similar to that reported by Jahr and Stevens (1990). The model NMDA current is thus

$$g(t) \times \frac{1}{1 + \frac{[\text{Mg}^{2+}]}{3} \times \exp[-0.07(V - \xi)]} \times (V - 60),$$

where ξ is either 50 or 60 mV. We take $[\text{Mg}^{2+}]$ to be 2 mM, the external concentration often used in hippocampal slice experiments. The current-voltage relation of the NMDA current so simulated has the characteristic negative dip at potentials between rest and the EPSP equilibrium potential (Nowak et al. 1984), in the present case being a minimum at 40.5 mV positive to rest when $\xi = 60$ mV. QUIS postsynaptic conductances onto a given neuron that are caused by multiple presynaptic action potentials (arriving at the same time as each other, or at different times) add linearly. Likewise, NMDA postsynaptic conductances onto a given neuron, caused by multiple presynaptic action potentials, add linearly. In each cell, the total NMDA conductance saturates: it is not allowed to exceed a predetermined maximum value.

The equation for intracellular $[\text{Ca}^{2+}]$ in compartment i , χ_i , is as follows

$$\frac{d\chi_i}{dt} = -\phi_i I_{\text{Ca},i} - \beta_{\chi} \chi_i \quad (3)$$

where ϕ_i is a scaling constant (defined in the *Glossary* at the end of the INTRODUCTION), and $\beta_{\chi} = 0.075 = 1/13.33 \text{ ms}^{-1}$. Such a rapid time constant (13.33 ms) for decay of intracellular Ca is consistent with the time constants determined for the decay of optical Ca signals in fine Purkinje cell dendrites: ~ 20 ms (W. N. Ross, personal communication) or even less than this (Sugimori and Llinás 1990). A negative value for $I_{\text{Ca},i}$ in Eq. 3 corresponds to inward current.

We did not attempt to include all of the ionic currents that have been described in hippocampal neurons. For example, we did not include the M type of K current (Halliwell and Adams 1982), the so-called anomalous inward rectifier (Hotson et al. 1979), the slowly inactivating I_K reported by Storm (1988), or the persistent Na current reported by French et al. (1990). It is not possible for us to be certain of the consequences of these omissions until a new model is developed that includes these currents. All we can say is that certain cellular firing properties can be reproduced with a limited repertoire of currents.

Kinetics of the active channels

The general formalism derives from the Hodgkin-Huxley equations. Thus, if x_k is a membrane state variable for compartment k , and ψ_k is either V_k or χ_k (depending on x_k), then

$$\frac{dx_k}{dt} = \alpha_x(\psi_k)(1 - x_k) - \beta_x(\psi_k)x_k \quad (4)$$

Note that the rate functions α_x and β_x do not themselves depend on k in our model; that is, we need not write $\alpha_{x,k}$ or $\beta_{x,k}$. To emphasize: we assume that the kinetics of voltage-dependent membrane channels are the same in the dendrites as in the soma. This is an assumption of the model made for the sake of simplicity and because of the lack of kinetic data on dendritic ionic channels.

The reader will recall the steady-state value of x , $x_\infty = \alpha_x/(\alpha_x + \beta_x)$ and the time constant for relaxation to x_∞ , $\tau_x = 1/(\alpha_x + \beta_x)$. Thus, if x_∞ and τ_x are known as functions of voltage, then the rate functions α_x and β_x can be reconstructed.

The rate functions that we use are shown in Tables 1 and 2. Some justification and comments on these rate functions now follow.

1) g_{Na} . Our m_∞ and h_∞ are similar to the steady-state "activation" and "inactivation" variables plotted by Sah et al. (1988a), allowing for the fact that $h(V)$ shifts to the right on the voltage axis at higher temperature (Sah et al. performed their experiments on isolated cells at 22°C, whereas most slice experiments are performed at $\geq 32^\circ\text{C}$). The rate functions for m and h were scaled so that dV/dt during an action potential was ≥ 100 V/s with $\bar{g}_{\text{Na}} = 30$ mS/cm² on the soma.

2) g_{Ca} . α_s and β_s are taken directly from Kay and Wong (1987) (our activation variable s is called "m" in that paper; we have also corrected printing errors in the equations of Kay and Wong). Our model resting potential, called "0 mV" in our mathematical notation, is assumed to correspond to -60 mV. Note that this calcium current is of the high-voltage-activated type. Although we are aware of data suggesting the existence of multiple types of calcium channels in CA3 cells (Fisher et al. 1990), the high-voltage-activated type is both the best characterized and is sufficient to account for depolarizing afterpotentials (DAP) and for bursting. The second power of the activation variable (s^2) is also taken from Kay and Wong (1987). The inactivation of g_{Ca} is complicated (Kay 1991), having fast and slow voltage-dependent phases and a calcium-dependent component as well. Because the slow voltage-dependent inactivation process and the calcium-dependent inactivation process take so long (τ of hundreds of milliseconds or more), we have omitted these processes. We approximate the fast inactivation with kinetics such that $r_\infty = 1$ at potentials hyperpolarized to rest and such that r_∞ is proportional to $e^{-V/20}$ for V above resting potential.

TABLE 1. Activation variable rate functions

Channel/Variable	Forward (α)	Backward (β)
g_{Na}/m	$0.32(13.1 - V)$ $\exp\left(\frac{13.1 - V}{4}\right) - 1$	$0.28(V - 40.1)$ $\exp\left(\frac{V - 40.1}{5}\right) - 1$
g_{Ca}/s	$\frac{1.6}{1 + \exp(-0.072(V - 65))}$	$0.02(V - 51.1)$ $\exp\left(\frac{V - 51.1}{5}\right) - 1$
$g_{\text{K(DR)}}/n$	$\frac{0.016(35.1 - V)}{\exp\left(\frac{35.1 - V}{5}\right) - 1}$	$0.25 \exp\left(\frac{20 - V}{40}\right)$
$g_{\text{K(AHP)}}/q$	$\min(0.2 \times 10^{-4}x, 0.01)$	0.001
$g_{\text{K(C)}}/c$	$\exp\left[\left(\frac{V - 10}{11}\right) - \left(\frac{V - 6.5}{27}\right)\right]$ 18.975	$2 \times \exp\left(-\frac{(V - 6.5)}{27}\right)$ $- \alpha_c \quad [V \leq 50]$
$g_{\text{K(A)}}/a$	$2 \times \exp\left(-\frac{(V - 6.5)}{27}\right)$	0 [$V > 50$]
		$0.02(13.1 - V)$ $\exp\left(\frac{13.1 - V}{10}\right) - 1$
		$0.0175(V - 40.1)$ $\exp\left(\frac{V - 40.1}{10}\right) - 1$

For abbreviations see *Glossary*.

TABLE 2. Inactivation variable rate functions

Channel/Variable	Forward (α)	Backward (β)
g_{Na}/h	$0.128 \exp\left(\frac{17 - V}{18}\right)$	$\frac{4}{1 + \exp\left(\frac{40 - V}{5}\right)}$
g_{Ca}/r	0.005	$0 \quad [V \leq 0]$ $\frac{\exp(-V/20)}{200} \quad [V > 0]$
$g_{\text{K(A)}}/b$	$0.0016 \exp\left(\frac{-13 - V}{18}\right)$	$\frac{0.05}{1 + \exp\left(\frac{10.1 - V}{5}\right)}$

Note: we are assuming that $r_\infty = 1$ if $V < 0$; otherwise $r_\infty = e^{-V/20}$, with $\tau \sim 200$ ms. For abbreviations see *Glossary*.

3) $g_{\text{K(DR)}}$. n_∞ and τ_n are close to those reported by Sah et al. (1988b), except that τ_n has been shifted to the right on the voltage axis by ~ 15 mV, in accord with data obtained from isolated CA3 cells (Numann et al. 1987) [the data of Sah et al. (1988b) were from isolated CA1 cells]. The use of the first power of n , rather than the usual higher powers, is also taken from Sah et al. (1988b). We did not include inactivation of this current. By using a higher power of n , it was possible to obtain narrower and larger action potentials than occur in the model as presented. We nevertheless chose to adhere to the formalism published by Sah et al. (1988b).

4) $g_{\text{K(A)}}$. a_∞ and b_∞ are consistent with the data of Numann et al. (1987, Fig. 4). The rate functions were scaled to be consistent with the few points given by these authors for τ_a and the point for τ_b (25 ms at -10 mV absolute potential).

5) $g_{\text{K(AHP)}}$. The forward rate function is calcium dependent but not voltage dependent (Lancaster and Adams 1986). It is scaled so that after a burst the peak AHP conductance is delayed for 100–200 ms (Lancaster and Adams 1986). The backward rate function, $1/1,000 \text{ ms}^{-1}$, is somewhat faster than the $1/2,000 \text{ ms}^{-1}$ reported by Numann et al. (1987), allowing for the temperature difference.

6) $g_{\text{K(C)}}$. We could not find sufficient data from hippocampal neurons to characterize the kinetics of this current, although it is known to be present in hippocampal neurons (Numann et al. 1987; Storm 1987). We therefore used data from Adams et al. (1982) from bullfrog sympathetic neurons. The conductance is increased by intracellular calcium. We assumed the conductance was proportional to a voltage-dependent term times a saturating calcium-dependent term. [This formalism is different from that of Yamada et al. (1989), who made the forward rate function dependent on both V and calcium]. A linear dependence of equilibrium $g_{\text{K(C)}}$ on intracellular calcium is consistent with data from *Aplysia* neurons, although in the latter case a dependence of channel kinetics on calcium seems likely (Zucker 1989). Furthermore, Zucker (1989) did not observe a saturation of the K current for intracellular calcium concentrations up to 20 μM , but this was under conditions in which calcium was released from an intracellular chelator by flash photolysis, rather than under physiological conditions. Adams et al. (1982) noted that τ_c increased e -fold for 27 mV of depolarization, that c_∞ increased e -fold for 11 mV of depolarization, and that c_∞ saturates abruptly (at a potential we take as 50 mV positive to rest). Our kinetics are the simplest that we could construct that are consistent with these data. The rate functions were scaled so that τ_c was fast enough for the conductance to be partially activated during a single action potential ($\tau_c = 3.62$ ms at 60 mV relative to rest). We did not include inactivation of this current.

Ionic conductance densities

This study proceeded in two phases. First was a general exploration of the effects of different soma-dendritic distributions of ionic conductance densities, together with some fine-tuning of the rate functions and the ϕ_i (i.e., the coupling of I_{Ca} to intracellular Ca concentration). We shall not describe this exploration in great detail, but rather present two particular sets of conductance densities, for CA3 and CA1 pyramidal cells, respectively (Tables 3 and 4; Figs. 1 and 2). The second phase was a detailed examination of the properties of the CA3 and CA1 models with fixed parameters. These properties will be presented in RESULTS.

Figure 3 shows the current-voltage relations for three of the model compartments. These curves reflect both the voltage- and calcium-dependent kinetics and the conductance densities. It is customary to present current-voltage relations in the steady state, when all of the membrane state variables have assumed their equilibrium values. For understanding bursting, however, we have found it more useful to use a pseudo-steady state in which all of the membrane state variables are in equilibrium except for one of the slowest ones, r (representing g_{Ca} inactivation); r is assumed to be 1. The reason for doing this is as follows. The current-voltage relation provides physical insight if one can approximate the membrane dynamics at a particular membrane voltage as an approach to the steady-state characteristic of that voltage, even though membrane currents keep changing the membrane voltage. In the "true" steady state of the model, g_{Ca} is largely inactivated at depolarized membrane potentials. Thus the steady-state approximation is not appropriate for the understanding of bursting, which critically depends on the occurrence of calcium-dependent action potentials taking place from a state without g_{Ca} inactivation. On the other hand, a typical burst of action potentials itself leads to negligible g_{Ca} inactivation, because the time constant of g_{Ca} inactivation is long relative to the depolarized part of a burst. The approximation $r = 1$ is therefore appropriate in this context. (Were a low-threshold Ca current to be included in the model, this approach would become more complicated.) We plot the current-voltage relation at a number of different "clamped" values of χ , the intracellular Ca concentration. These different χ values determine the extent to which $g_{K(C)}$ and $g_{K(AHP)}$ are activated. The cusps that occur in some of the curves at 50 mV positive to rest reflect the postulated sudden saturation of $g_{K(C)}$ at this potential.

TABLE 3. Ionic conductance densities (mS/cm^2) for CA3 cell model

Compartment	g_{Na}	g_{Ca}	$g_{K(DR)}$	$g_{K(AHP)}$	$g_{K(C)}$	$g_{K(A)}$	g_L
1	0.0	0.0	0.0	0.0	0.0	0.0	0.1
2	0.0	5.0	0.0	0.8	5.0	0.0	0.1
3	0.0	5.0	0.0	0.8	5.0	0.0	0.1
4	0.0	12.0	0.0	0.8	10.0	0.0	0.1
5	0.0	12.0	0.0	0.8	10.0	0.0	0.1
6	20.0	12.0	20.0	0.8	10.0	0.0	0.1
7	0.0	5.0	0.0	0.8	5.0	0.0	0.1
8	15.0	8.0	5.0	0.8	20.0	0.0	0.1
9 (soma)	30.0	4.0	15.0	0.8	10.0	5.0	0.1
10	15.0	8.0	5.0	0.8	20.0	0.0	0.1
11	0.0	5.0	0.0	0.8	5.0	0.0	0.1
12	20.0	17.0	20.0	0.8	15.0	0.0	0.1
13	0.0	17.0	0.0	0.8	15.0	0.0	0.1
14	0.0	17.0	0.0	0.8	15.0	0.0	0.1
15	0.0	10.0	0.0	0.8	15.0	0.0	0.1
16	0.0	10.0	0.0	0.8	15.0	0.0	0.1
17	0.0	5.0	0.0	0.8	5.0	0.0	0.1
18	0.0	5.0	0.0	0.8	5.0	0.0	0.1
19	0.0	0.0	0.0	0.0	0.0	0.0	0.1

For abbreviations see Glossary.

TABLE 4. Ionic conductance densities (mS/cm^2) for CA1 cell model

Compartment	g_{Na}	g_{Ca}	$g_{K(DR)}$	$g_{K(AHP)}$	$g_{K(C)}$	$g_{K(A)}$	g_L
1	0.0	0.0	0.0	0.0	0.0	0.0	0.1
2	0.0	5.0	0.0	0.8	5.0	0.0	0.1
3	0.0	5.0	0.0	0.8	5.0	0.0	0.1
4	0.0	7.0	0.0	0.8	5.0	0.0	0.1
5	0.0	7.0	0.0	0.8	5.0	0.0	0.1
6	20.0	12.0	20.0	0.8	10.0	0.0	0.1
7	0.0	5.0	5.0	0.8	5.0	0.0	0.1
8	15.0	8.0	10.0	0.8	20.0	0.0	0.1
9 (soma)	30.0	4.0	25.0	0.8	10.0	5.0	0.1
10	15.0	8.0	10.0	0.8	20.0	0.0	0.1
11	0.0	5.0	5.0	0.8	5.0	0.0	0.1
12	20.0	17.0	20.0	0.8	15.0	0.0	0.1
13	0.0	7.0	0.0	0.8	5.0	0.0	0.1
14	0.0	7.0	0.0	0.8	5.0	0.0	0.1
15	0.0	7.0	0.0	0.8	5.0	0.0	0.1
16	0.0	5.0	0.0	0.8	5.0	0.0	0.1
17	0.0	5.0	0.0	0.8	5.0	0.0	0.1
18	0.0	5.0	0.0	0.8	5.0	0.0	0.1
19	0.0	0.0	0.0	0.0	0.0	0.0	0.1

Numerical methods. The differential equations were integrated using a 2nd-order Taylor series method (Daniel and Moore 1970; Traub and Miles 1991b) with a fixed time step of 50 μs . Programs were written in FORTRAN and run on an IBM 3090 computer. For making figures, data were stored every 0.25 ms of a simulation.

Several features of the current-voltage relations are worthy of note. The soma has a "well" of inward current at 25 mV positive to rest, as a result of g_{Na} . The relatively small g_{Ca} appears as an inflection on the current-voltage curve at 60 mV when χ is small. In contrast, at 0.3 λ from the soma, there are two distinct wells, one for g_{Na} and one for g_{Ca} , with the latter disappearing as χ is increased. We remind the reader that g_{Ca} inactivation was not included in this figure, so that disappearance of the g_{Ca} well with increasing χ is caused by activation of $g_{K(C)}$. One expects that Na

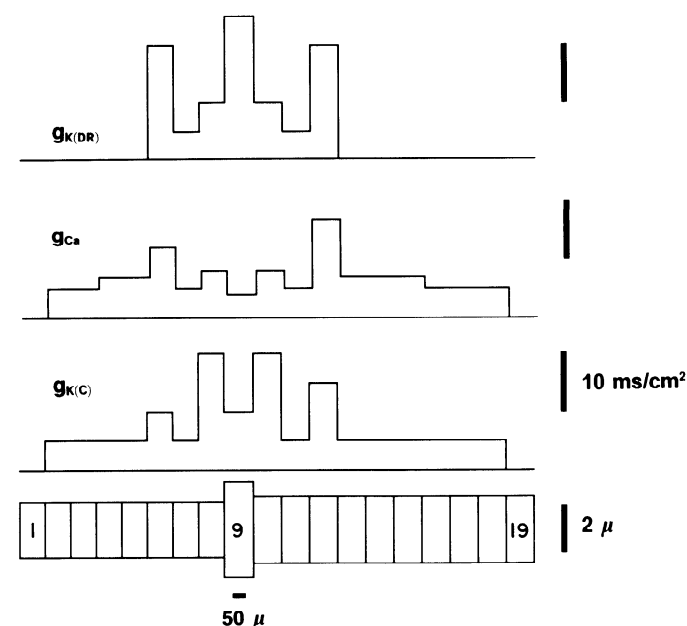


FIG. 2. Densities of 3 of the ionic conductances in the CA1 pyramidal cell model. Density for g_{Na} is the same as in the CA3 model. Electrotonic architecture (below) is also the same.

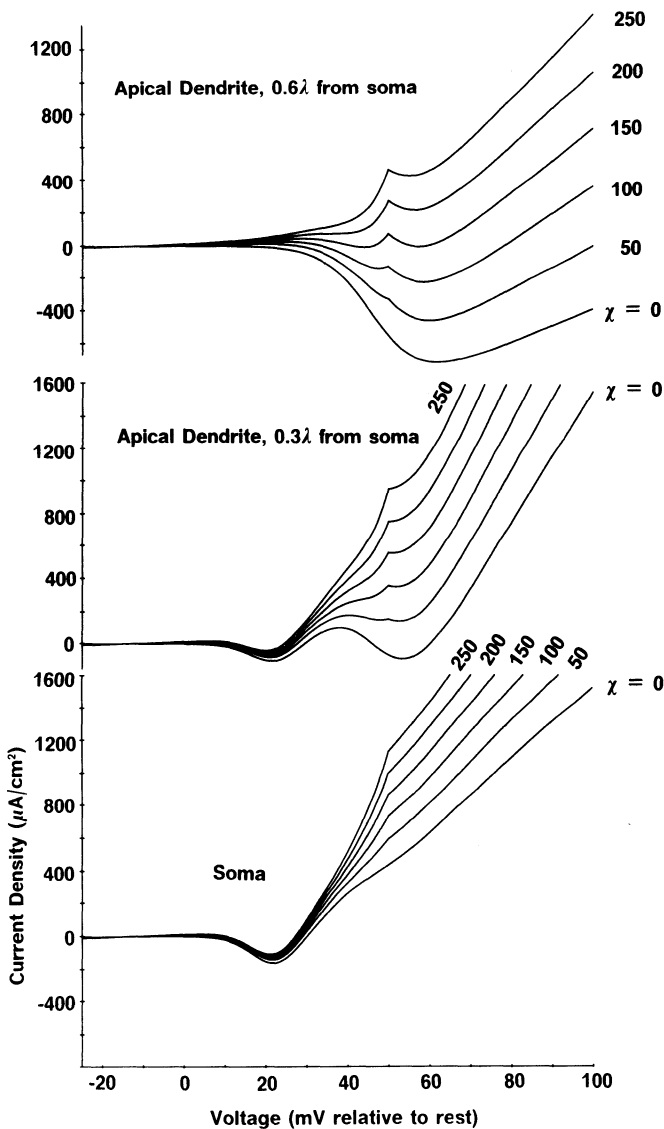


FIG. 3. Current-voltage relations for 3 different compartments in the CA3 model, plotted for 6 different values of χ (submembrane Ca concentration). All ionic conductances assume their steady-state value at each voltage, except that $r = 1$ (i.e., there is no inactivation of g_{Ca}).

spikes would occur readily at this dendritic location but that Ca spikes would occur only in a "resting" condition of low intracellular Ca. Finally, at 0.6λ from the soma, g_{Na} is absent. There is a large I_{Ca} well corresponding to the high g_{Ca} density; this well persists until $\chi > 150$, reflecting the absence of $g_{\text{K}(\text{DR})}$ in this region of the model membrane. One expects, therefore, that repetitive Ca spikes might be generated here, provided that membrane potential can be held depolarized enough and that at the same time the cell is not too overloaded with Ca. A rapid time constant for removal of intracellular calcium (i.e., a large value of β_x) favors the occurrence of repetitive calcium spikes.

Some of the justification for the conductance densities is as follows. These comments apply to our CA3 model.

1) g_{Na} . The data of Sah et al. (1988a) indicate that the density of this conductance in an isolated cell can be as high as $40 \text{ mS}/\text{cm}^2$. For both CA3 and CA1 models, we use a density of $30 \text{ mS}/\text{cm}^2$ on the soma and a somewhat smaller density on the adjacent membrane. Because the apical dendrites in CA1 and CA3 cells (Masukawa and Prince 1984; Wong et al. 1979) can generate Na spikes, as can CA1 basilar dendrites (Lacaille et al. 1987), we have a com-

partment in each dendritic cylinder with sufficient g_{Na} to generate an action potential ($20 \text{ mS}/\text{cm}^2$).

2) g_{Ca} . The density of g_{Ca} was estimated by Kay and Wong (1987) to be $\sim 7 \text{ mS}/\text{cm}^2$ in isolated CA1 cells. We have kept g_{Ca} density near to this value on and next to the soma, the average density on the soma and adjacent compartments being $6.15 \text{ mS}/\text{cm}^2$. If this density is too large at the soma, action potentials become too broad or do not repolarize. At the same time, there must be sufficient g_{Ca} on and near the soma so that burstlike events (usually without slow Ca-mediated action potentials) can occur in isolated cells as illustrated in Fig. 4. In the model, g_{Ca} is critical for generation of the depolarizing envelope of such bursts. Intradendritic recordings from isolated dendrites (Masukawa and Prince 1984) and from whole cells (Poolos et al. 1990; Wong et al. 1979; Michelson and Wong, unpublished data) indicate that calcium spikes and bursts can be generated in the dendrites independent of the soma. This is the case in both CA1 and CA3 cells. Calcium spikes may be as large as 65 mV and are larger in the middle dendrites than in the soma (Wong et al. 1979). Calcium-imaging

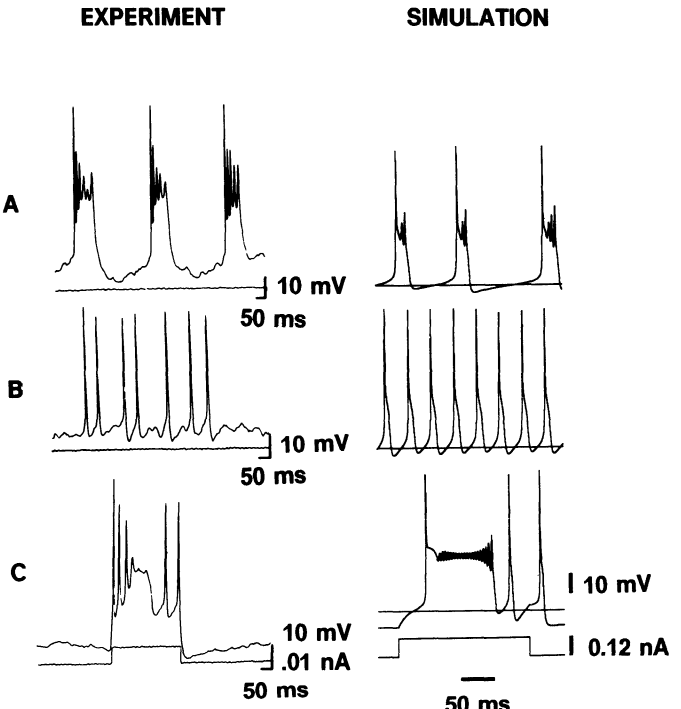


FIG. 4. Bursts and repetitive firing in acutely isolated CA3 neuron (Experiment, left) and in model isolated cell containing soma and 1 basilar and 1 apical compartment (Simulation, right). In the experiment, the whole-cell recording electrode contained 11 mM ethylene glycol-bis (β -aminoethyl ether)- N,N,N',N' -tetraacetic acid (EGTA) to block Ca-dependent currents. In the model, $\bar{g}_{\text{K}(\text{C})}$ and $\bar{g}_{\text{K}(\text{AHP})}$ were each reduced 20-fold. Passive membrane properties in the model were not altered to agree with the much higher R_m and smaller C_m of the isolated cell. Experimental traces are A: spontaneous bursts; B: repetitive single action potentials (different cell); C: burst in the same cell as B; the cell was held hyperpolarized and then a sustained depolarizing pulse delivered. Model traces: A: repetitive bursting during passage of steady 0.015-nA current into soma. B: rhythmic action potentials during passage of 0.1-nA current into soma. C: cell was hyperpolarized with a steady -0.05 nA current, and then a 0.07 nA current pulse was applied; current trace below. Note that g_{Ca} appears to be activated faster than in the corresponding experimental trace, and it produces a plateau rather than a discrete slow action potential. Horizontal lines in simulation traces mark the resting potential; they mark injected current in experimental records. Noise in experimental traces may be caused by spontaneous openings of single membrane channels, the effect of this being apparent because of the very high input resistance of the isolated cell, up to $1,000 \text{ M}\Omega$ (Kay and Wong 1986).

experiments likewise indicate the existence of voltage-dependent g_{Ca} channels in basilar and apical dendrites (Regehr et al. 1989), although perhaps not in the most extreme distal dendrites. We have therefore placed sufficient g_{Ca} in both sets of dendrites so that large calcium spikes can be locally generated (see later). By modifying the amount of dendritic g_{Ca} together with somatic $g_{K(DR)}$, we can regulate how the cell responds to somatic injection of current: either with bursting or with trains of action potentials.

3) $g_{K(DR)}$. Although several outward currents may contribute to repolarization of the action potential (Storm 1987), $g_{K(DR)}$ should be sufficient to repolarize the action potential unassisted at least in an isolated CA1 cell (Sah et al. 1988b). We chose to follow Sah et al. (1988b) in this respect. If $g_{K(DR)}$ density is too small, the action potential becomes too broad or does not repolarize at all; if the density is too large, the action potential is too small or there is a large immediate AHP (although this latter might be masked by I_{Ca}). Because the model contains regions of dendritic g_{Na} , $g_{K(DR)}$ must be located in the dendrites to repolarize dendritic Na action potentials. On the other hand, significant $g_{K(DR)}$ in the more distal dendrites would suppress the generation of Ca spikes. This in turn meant that $g_{K(C)}$ was the main outward current for repolarization of calcium spikes. This current was especially important because the voltage-dependent inactivation of I_{Ca} is slow.

4) $g_{K(C)}$. The density of this conductance approximately followed that of g_{Ca} to ensure repolarization of Ca spikes. The relative density of the two conductances was reflected in the width of the calcium spikes. Inclusion of additional dendritic K currents (e.g., M current, A current) might have altered the requisite balance between g_{Ca} and $g_{K(C)}$.

5) $g_{K(AHP)}$. A constant density was used (except where g_{Ca} was absent) sufficient that a post-burst AHP was in the range 5–10 mV.

6) $g_{K(A)}$ was located only at the soma, an assumption that may not be accurate. The density was sufficient to produce a characteristic lag in the response to a depolarizing current after the cell had been hyperpolarized for several hundred milliseconds (not shown). Although this current produced some effects on repetitive bursting (some prolongation of the interburst interval), its contribution to the model behavior appeared to be rather subtle. By “titrating” the density of $g_{K(A)}$, we noted that increasing this density led to a delay in onset of a current-evoked action potential, as well as to a smaller amplitude of the action potential. This implies that the current was activated on the upstroke of the action potential. Perhaps if we had used somewhat slower kinetics for this conductance, it might instead have made more contribution to action-potential repolarization.

Different Ca dynamics in the soma and dendrites

Assuming that C-current kinetics are the same in soma and dendrites, we then found it necessary to delay the coupling of Ca entry to C-current activation in the dendrites. This was necessary for the occurrence of large dendritic calcium spikes. Our finding may be an artifact of the C-conductance formalism that we use in that intracellular calcium is always in equilibrium with the conductance (because the conductance is proportional to x). We make the assumption that the dendritic shell in which calcium interacts with K channels is larger (by a factor of 4.44) than the corresponding shell for the soma and immediately adjacent compartments. The relevant parameter in the model is called ϕ_i (see the Glossary and Eq. 3). Thus more calcium entry must occur in the dendrites compared with the somatic region to raise x by the same extent. This assumption is equivalent formally to assuming stronger buffering of calcium in the dendrites than in the soma. The approach of Yamada et al. (1989) is an alternative one, whereby calcium is not in equilibrium with the C-channel but rather influences the kinetics of channel opening.

RESULTS

Somatic action potential

Figure 5 illustrates superimposed somatic action potentials generated by the whole neuron model under three different stimulation conditions: somatic injection of 0.1-, 0.4-, and 0.5-nA currents. The spikes are aligned at the point 10.5 mV depolarized to rest on the initial phase. The width of this spike at half-amplitude is 1.25 ms, somewhat wider than that observed by Miles (1990) (0.8 ms). This may be a reflection of too-slow DR kinetics in the model or of the model's use of first-power kinetics ($I_{K(DR)} \propto n$) rather than higher-power kinetics (such as $I_{K(DR)} \propto n^3$).

The spike afterpotential is sensitive to the stimulating conditions. A single spike evoked by an on-off current pulse may be followed by a DAP (see below and Fig. 6). On the other hand, spikes that occur from depolarized holding potentials are often followed by a brief AHP (see below and bottom 2 traces of Fig. 8).

Calcium dependence of the DAP and contribution of DAP to burst generation

Two important observations of Wong and Prince (1981) on CA3 cell bursts were these: a burst could sometimes be elicited by a brief depolarizing pulse, whereas the same pulse followed by a hyperpolarizing pulse could abort the burst, leaving instead a single spike followed by a DAP lasting some tens of milliseconds. The DAP, in turn, was shown to be in large part dependent on a calcium current. These behaviors also occur in our model (Fig. 6). On the left of Fig. 6, a depolarizing-hyperpolarizing current pulse is injected into the soma, eliciting an action potential. The electrotonically propagated response in the dendrites also

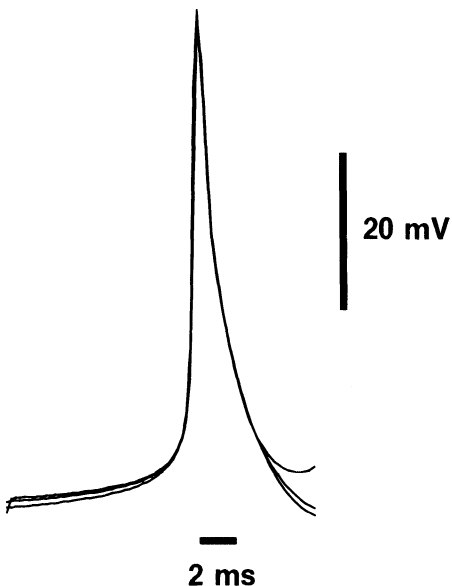


FIG. 5. Single action potentials in CA3 cell model at 3 different somatic bias currents (0.1, 0.4, and 0.5 nA). Action potentials were aligned at 10.5 mV positive to resting potential. Action potential peaks are all within 1 mV of each other. Afterpotentials do not reflect differences in intrinsic currents but rather the effect of the bias current, with a larger bias current associated with a more depolarized afterpotential.

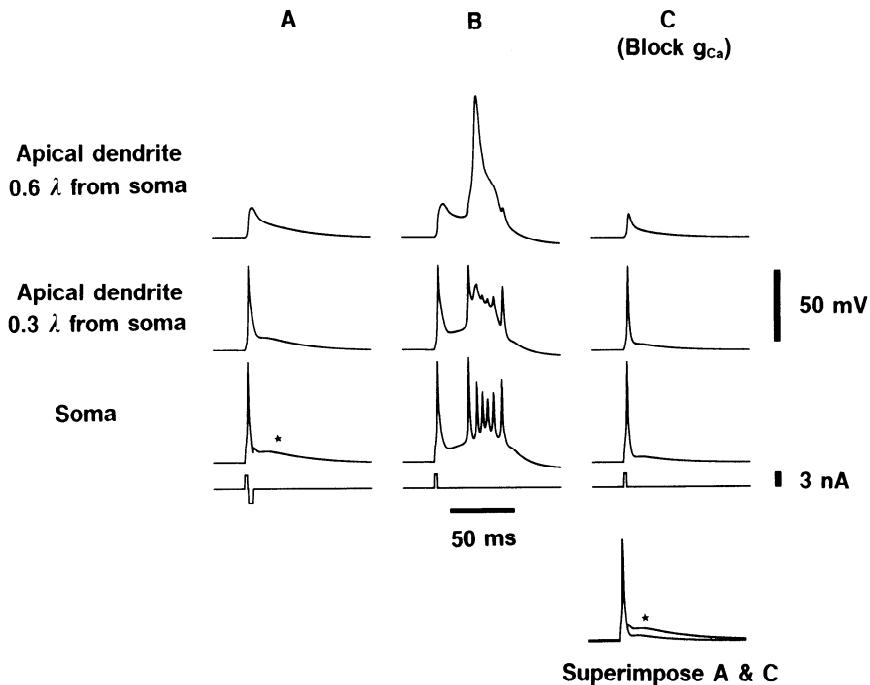


FIG. 6. Calcium dependence of the depolarizing afterpotential (DAP) and details of bursts initiated by somatic stimulation. *A*: a depolarizing/hyperpolarizing pulse (bottommost trace) elicits a somatic and proximal dendritic fast spike, but no Ca spike and no burst. Potential developing in the dendrite has, however, a slow regenerative (but subthreshold) component—compare the slow relaxation of the 0.6λ potential with the corresponding potential in *C* (where g_{Ca} is blocked). This slow Ca-dependent potential produces a spike DAP in the soma (*) and proximal dendrites. *B*: same depolarizing current as in *A*, without the hyperpolarizing current, allows the more distal dendrite to generate a full Ca spike, and the soma and proximal dendrites burst (compare Wong and Prince 1981). *C*: same stimulus was applied as in *B*, but with g_{Ca} blocked. Without g_{Ca} , a burst cannot develop, and the spike DAP is smaller than in *A* (somatic traces from *A* and *C* superimposed in bottom right inset).

contains a regenerative component, as is evident from its relatively large amplitude and slow relaxation (compare the top trace in Fig. 6*A* with the top trace in Fig. 6*C*, g_{Ca} having been blocked in the latter). The I_{Ca} so generated contributes in turn to the DAP, both in proximal dendrites and the soma (Fig. 6*A*, bottom 2 traces). The DAP, after a single spike with g_{Ca} blocked, is considerably smaller (Fig. 6*C*), even though the Na-spikes in soma and proximal dendrites are very close to the same amplitude. A residual DAP independent of g_{Ca} has been noted experimentally (Konnerth et al. 1986), and simulations in an earlier model suggested that the residual DAP was caused by discharging of dendritic capacitance originally charged by the Na spike (Traub 1982).

When only the depolarizing stimulus is given, the regenerative Ca event is just able to evoke a dendritic Ca spike (Fig. 6*B*) and hence a burst. In these near-threshold conditions, one can imagine that small dendritic membrane shunts or hyperpolarizations, such as might occur in the slice from dendritic inhibitory postsynaptic potentials (IPSPs), would prevent the complete burst. Note that, in the proximal dendrites, the burst contains both rapid and slower action potentials, as occurs experimentally (Fig. 6*B*, middle trace). Under conditions in which tonic-inhibitory shunts are present at the soma (to block action potentials) and in the middle dendrites (to block Ca spikes), single action potentials can be evoked at 0.3λ from the soma; these Na action potentials appear then at the soma as d-spikes (not shown) (Schwartzkroin 1977; Spencer and Kandel 1961).

Membrane events during a burst

Figure 7 provides insight into some of the membrane events during a burst (evoked by a steady current of 0.3 nA injected into the soma). We have plotted certain variables from the soma (left) and middle apical dendrite (right) at a location where g_{Ca} , $g_{K(AHP)}$, and $g_{K(C)}$ are the only active

conductances. Below the voltages (V) are plotted quantities that are proportional to the different active membrane conductances. Thus $g_{K(AHP)} \propto q$, $g_{K(DR)} \propto n$, $g_{K(C)} \propto c\chi$, $g_{Ca} \propto s^2r$, and $g_{Na} \propto m^2h$. The sequence of events during a burst, with these stimulating conditions, is as follows: a brief series of action potentials (2 in the present case) develops in the soma and propagates distally into the dendrites. The electrotonic potentials in the dendrites in turn evoke Ca electrogenesis that initially is subthreshold (see the 2 discrete humps in the right voltage trace of Fig. 7). The dendritic

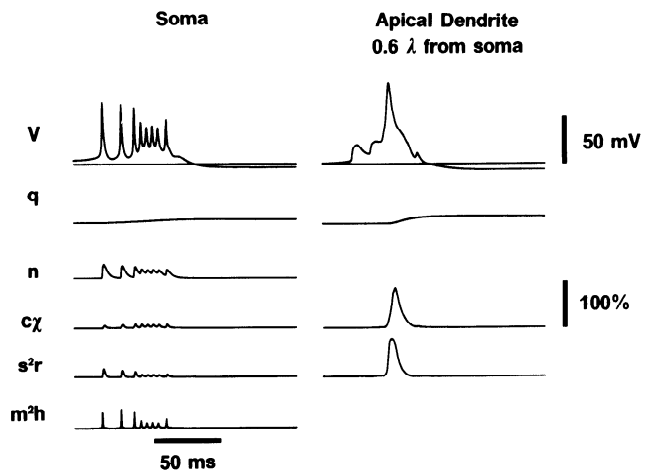


FIG. 7. State variables during a burst (CA3 cell model). Combinations of variables were chosen to which the different ionic conductances are proportional. Thus $g_{Ca} \propto q$, $g_{K(DR)} \propto n$, $g_{K(C)} \propto c\chi$ (provided χ remains below saturation; see Eq. 2), $g_{Ca} \propto s^2r$, and $g_{Na} \propto m^2h$. Burst occurred during injection of 0.3 nA current into the soma. Note the large dendritic Ca spike, with multiple components. First 2 Ca events follow somatic Na spikes whereas the large component of the Ca spike in turn contributes to the somatic burst envelope. A full Ca spike does not occur in the soma, although transient Ca currents flow (compare the s^2r signals at the 2 locations). Because $g_{K(DR)}$ and g_{Na} are absent 0.6λ from the soma in the model, n and m^2h are not shown on the right.

membrane, if depolarized sufficiently long and if not excessively shunted, can develop a large Ca spike (Fig. 7, right) that in turn propagates back to the soma and contributes to the depolarizing envelope of the burst. In contrast, somatic g_{Ca} does not contribute significantly to this envelope: note that somatic s^2r consists of a series of transient deflections rather than the sustained wave of g_{Ca} in the apical dendrite. Somatic action potentials are repolarized by both the DR (n) and the C-conductance ($\propto c_x$), with the DR being more activated (and also denser) at the soma. The burst is followed by a prolonged AHP. In the burst here illustrated, $g_{K(AHP)}$ is activated sooner and to a greater extent in the dendrites than at the soma. Our model did not produce slow Ca-dependent spikes at the soma; such events could be seen in the proximal dendrites, however (Fig. 6B).

Low-frequency rhythmic bursting and high-frequency repetitive action potentials

Another basic property of CA3 cells is that they express different modes of firing in response to steady injection of current into the soma, depending on the magnitude of the injected current (Wong and Prince 1981). For small depolarizing currents, rhythmic bursting at low frequency is observed, whereas for large injected currents, only rhythmic single action potentials (or small groups of spikes) are seen. Hablitz and Johnston (1981) studied burst frequency as a function of membrane potential. Over the range -59 to -51 mV, burst frequency increased from ~ 0.28 to ~ 1.0 Hz. Figure 8 demonstrates that our model also exhibits this type of behavior. The bursting induced by injection of currents <0.2 nA is stable and rhythmic. Likewise, for injected currents of ≥ 0.5 nA, the initial burst is a transient, whereas the repetitive firing is stable and persistent. More complicated behaviors are observed at intermediate currents, consisting of full bursts (with dendritic Ca spikes and prominent AHPs) intermixed with brief runs of spikes that are on occasion followed by a small AHP (as in the 0.3-nA trace in Fig. 8). Similar types of intermediate behav-

iors are seen experimentally, although for cells in the slice one can see more action potentials between bursts than occurs in the model. In the model, such a brief run of spikes, as "recorded" at the soma, is not associated with a dendritic Ca spike (not shown); this is the reason that a full AHP does not follow the brief train.

Third firing mode: rhythmic dendritic Ca spikes

The firing modes illustrated in Fig. 8 are known to occur experimentally. The model predicts the occurrence of another mode of firing behavior when a compartment in the middle or distal dendrites is excited tonically (Fig. 9). In this third mode, repetitive calcium spikes are generated, each being correlated with a brief burst of action potentials at the soma. Figure 9 depicts some of the mechanisms underlying these different firing modes. 1) With a small somatic depolarizing current (Fig. 9, left), a large and prolonged AHP follows a burst. Because of the small stimulus, no somatic action potentials occur until the AHP has diminished sufficiently. When somatic action potentials finally do occur, they are able to propagate back to the dendrites and elicit regenerative g_{Ca} . 2) During the injection of large somatic currents (Fig. 9, middle), the stimulus is strong enough to elicit somatic action potentials in spite of the local dendritic membrane shunt from $g_{K(AHP)}$ and other outward currents. When these spikes propagate into the dendrites, they find the dendritic membrane too shunted to permit full Ca electrogenesis. Nevertheless, enough Ca entry still occurs to maintain the dendritic shunt via $g_{K(AHP)}$ and $g_{K(C)}$. This pattern is stable and so rhythmic firing continues. 3) During injection of large depolarizing current into the dendrites, the local membrane shunt is overcome. In the model, fast spikes are initiated in the soma in these conditions (Fig. 9, right), propagating distally to initiate Ca spikes. The sustained dendritic depolarization allows this process to occur at much higher frequencies than will be seen during bursting caused by somatic stimulation. In the latter case, the long AHP limits the frequency because of the dendritic shunt. In the case of dendritic stimulation, the frequency is limited by more rapid processes, including the time constant for removal of Ca from the submembrane shell (13.33 ms in the present model).

How much cell membrane is required to observe the transition from repetitive bursting to rhythmic single action potentials?

Given a set of ionic conductance densities and membrane kinetics, one can ask how much cell membrane is necessary to generate a transition from bursting to repetitive firing. We addressed this question in the model by disconnecting progressively larger pieces of the distal apical and basilar dendrites; in each case, a range of currents was then injected into the soma. The transition from bursting to repetitive firing shown in Fig. 8 was little altered when the basilar dendrites were 0.6λ and the apical dendrites were also 0.6λ in electrotonic length. However, the case was different with much shorter dendrites. For example, when each set of dendrites was only 0.4λ , the cell would generate only bursts until the current was large enough (1.0 nA) to drive the membrane into a sustained steady depolarization.

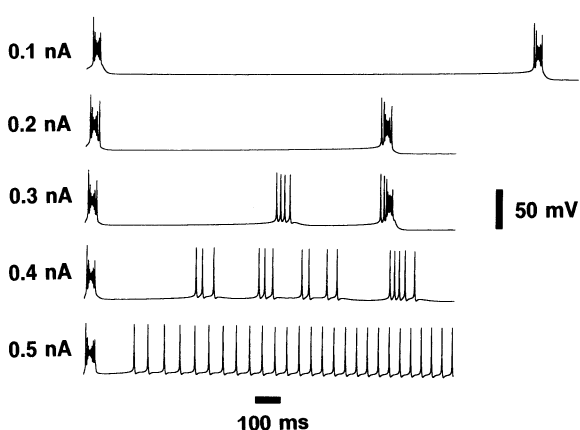


FIG. 8. Different firing modes of the CA3 model during tonic depolarizing stimulation at the soma. For smaller stimulating currents, the cell generates rhythmic bursts at low frequency (see also Fig. 10). At somewhat higher currents (e.g., 0.3 nA) rhythmic bursts occur, but with intercalated runs of fast spikes; these runs have little depolarizing envelope, a small AHP, and no concurrent dendritic Ca spike (not shown). At sufficiently large currents (e.g. 0.5 nA), after an initial burst, the cell settles into rhythmic single action potentials (see also Fig. 10).

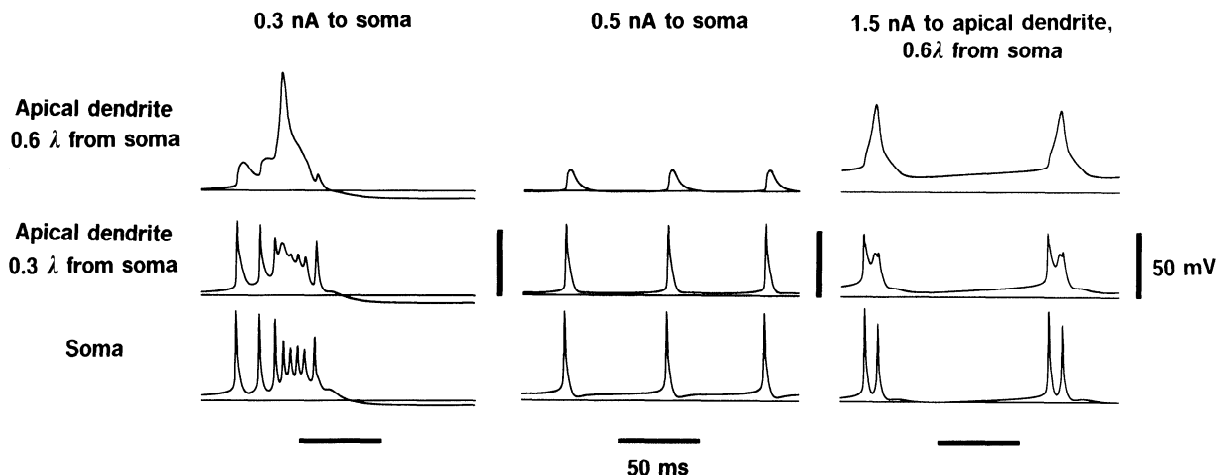


FIG. 9. Events in different membrane regions help to explain why different firing modes exist. Maintained currents were applied to different membrane regions of the CA3 model. *Left*: burst initiated by somatic current injection begins with somatic action potentials. These propagate distally. Provided that the dendrite is not too hyperpolarized or shunted (which will be true if no firing has taken place for >1 s), the induced dendritic depolarization can become fully regenerative. This in turn leads to a burst more proximally and in the soma itself. *Middle*: with a larger somatic injected current, somatic spikes are induced despite the membrane shunt. Distal dendritic membrane is too shunted for full Ca spikes to develop, but enough subthreshold Ca current flows to maintain the shunt. *Right*: injection of a large current directly into the dendrite allows dendritic Ca spikes to occur despite the local membrane shunt. Note that, even with dendritic stimulation, each calcium spike is initiated by a Na spike in the soma/proximal dendrites.

As the injected current was increased up to 0.8 nA in the cell fragment, the average frequency of bursts increased, and long (~ 200 ms) bursts became intermixed with short bursts containing as few as two action potentials. Runs of single action potentials were not sustained more than ~ 100 ms. The exact dendritic length at which the bursting/repetitive firing transition becomes blurred or lost is clearly sensitive to the distribution of outward current densities. For example, if the densities of $g_{K(C)}$ and $g_{K(AHP)}$ are each reduced 20-fold, then even the model "isolated soma" (soma with an attached basilar and apical compartment) can exhibit a burst/repetitive firing transition as injected current is increased (Fig. 4).

Rhythmic dendritic Ca spikes might be relevant to hippocampal physiology in the following way. Because afferents to hippocampal neurons tend to be laminated, it is

possible that CA3 recurrent excitatory inputs to any given pyramidal cell might impinge on relatively discrete regions of the apical and basilar dendrites (Ishizuka et al. 1990). Therefore, during a synchronized burst occurring during blockade of GABA_A synapses (Miles et al. 1984), discrete dendritic regions might be excited in an intense but basically physiological manner. This excitation could elicit repetitive calcium spikes. We shall return to this issue later in the context of synchronized multiple bursts.

Quantitative aspects of three modes of firing

Figures 10 and 11 summarize, in the form of frequency-current (f/I) curves, the three different firing modes presented above. Figure 10, *left*, shows that low-frequency bursting occurs over the same frequency range as observed experimentally by Hablitz and Johnston (1981), ~ 0.3 –1.0

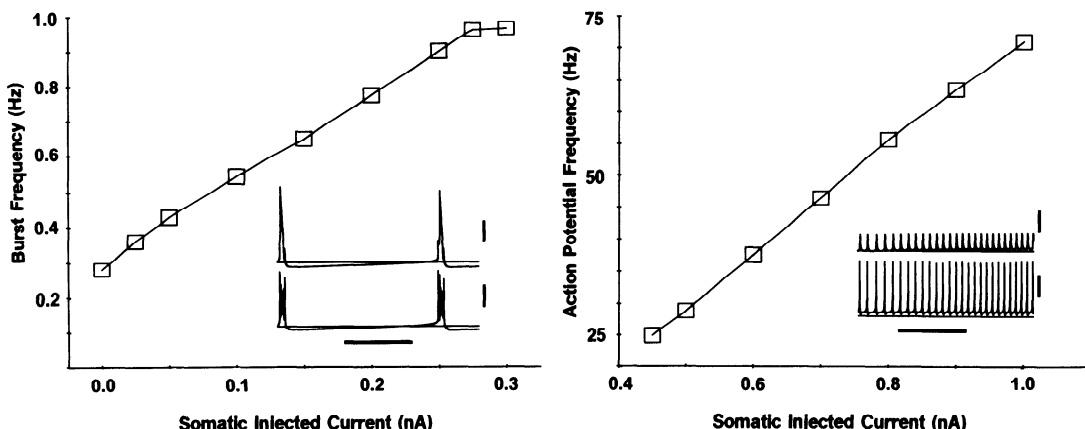


FIG. 10. Frequency-current (f/I) curves for 2 firing modes induced by somatic current injection. CA3 model. Note the different frequency ranges. Burst frequencies correspond to those observed experimentally (Hablitz and Johnston 1981). We did not count action potentials during repetitive bursting to derive mean action potential rate during repetitive bursting. Insets: representative voltage tracings for the 2 firing modes; bottom trace is somatic potential and top trace is potential in the apical dendrite 0.6λ from the soma. Calibrations for insets are 25 mV and 500 ms.

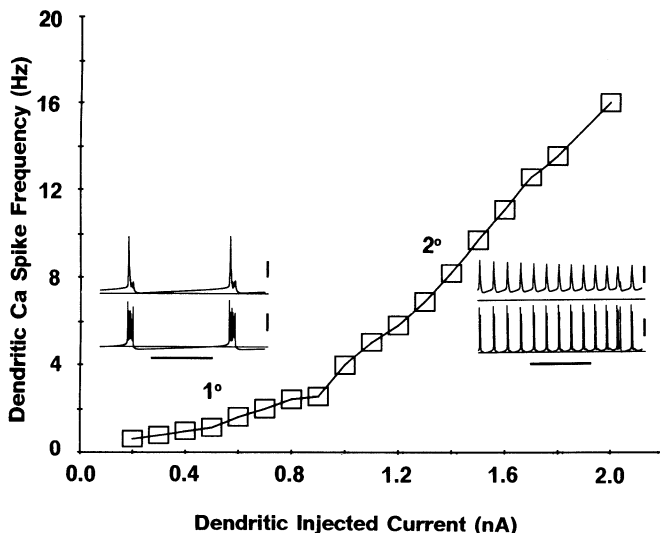


FIG. 11. f/I curve in CA3 cell model for dendritic current injections. Bursting can now be induced at frequencies observed during synchronized multiple bursts. Note the 1 and 2° ranges in the curve, an interesting feature to check experimentally. Insets: representative voltage tracings for the 1 and 2° ranges; bottom trace is somatic potential and top trace is potential in the apical dendrite 0.6λ from the soma. Calibrations for insets are 25 mV and 500 ms.

Hz. Repetitive action potentials elicited by somatic depolarization occur with minimum frequency at ~ 25 Hz, and the frequency increases at ~ 80 Hz/nA (Fig. 10, right); we are not aware of experiments that determine this frequency-dependence quantitatively. With somatically injected current of 1.4 nA and above, the soma enters a state of depolarization block (not shown). The f/I curve for dendritic injection of depolarizing current exhibits a primary and secondary range (Fig. 11). This probably reflects the fact that low-frequency bursting is limited by the AHP duration, whereas high-frequency bursting takes place superimposed on an approximately constant AHP membrane shunt. The frequency in the latter case should then be determined by the kinetics of the $g_{Ca}-\chi-g_{K(C)}$ system. For sufficiently large dendritic injected currents, the dendritic membrane enters a state of sustained depolarization (not shown).

We shall now consider briefly our CA1 pyramidal cell model. Recall that the kinetics of the membrane currents and of submembrane calcium (χ) in this model are the same as in the CA3 model, but that the distribution of conductance densities is different (Table 4; Fig. 2). The different conductance distribution affects the simulated CA1 spike afterpotential (not shown): there is a transient (5–10 ms) spike AHP before a small DAP that lasts ~ 20 ms.

CA1 cell model firing behavior depends on site of stimulation

A range of different steady currents was injected into different regions of the CA1 cell model. Figure 12 illustrates the behavior when a steady depolarizing current of 0.25 nA was injected either into the soma (left) or 0.3 or 0.6λ into the apical dendrite away from the soma. For currents < 1 nA injected into the soma, rhythmic trains of action potentials occur (Fig. 12, left), associated in the distal dendrites with a tonic depolarization and superimposed subthreshold

voltage transients. [Large currents, ≥ 1.15 nA, cause higher-frequency firing in which is embedded a burst with a depolarizing envelope, lacking a significant AHP (not shown). A transient initial acceleration of firing is seen in the slice also in CA1 cells stimulated with large currents (see the raster plots of Lanthorn et al. 1984).] Stimulation at 0.3λ from the soma elicits behavior similar to that seen when the soma itself is excited (Fig. 12, middle), although the distal dendritic depolarization is now larger. Finally, stimulation further out in the dendrites (Fig. 12, right) elicits a full calcium spike associated with a somatic burst, as occurs experimentally (Wong and Traub 1982). Note that the somatic depolarizing burst envelope is small in this case. We should point out that, unlike in the CA3 model, the dendritic calcium spike so elicited in our model does not recur rhythmically during a sustained depolarizing dendritic current. Rather, the calcium spike is followed by a pause of ~ 1 s, after which rhythmic somatic action potentials occur (not shown).

Quantitative aspects of CA1 cell repetitive firing

The f/I plot for our model CA1 cell is shown in Fig. 13. At stimulating currents > 0.25 nA, the plot is roughly linear. In the adapted state, the slope is 74 Hz/nA, somewhat larger than reported by Lanthorn et al. (1984), who give average values of 34.1 and 19.7 Hz/nA, respectively, for the two classes of CA1 cells that they distinguish. Note the lack of adaptation between the first and second interspike intervals in the model, in contrast to experimental data (Lanthorn et al. 1984; Schwartzkroin 1978). This occurs in the model because of the rapid development of a tonic dendritic depolarization (Fig. 12) that initially accelerates firing before the AHP current develops enough to slow down the firing.

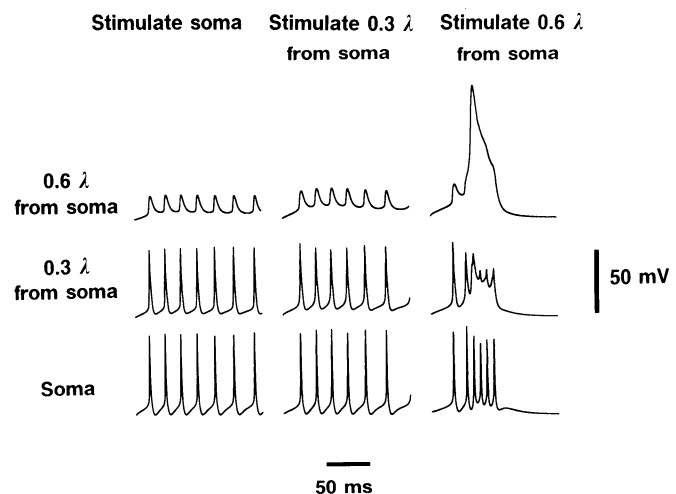


FIG. 12. CA1 cell model: different responses for somatic and dendritic stimulation. A constant current (0.25 nA in each case) was injected into 1 of 3 different locations. During injection into the soma or into a site 0.3λ out in the apical dendrites (left and middle, respectively), repetitive firing is elicited. This repetitive firing is superimposed, in the dendrites, on a tonic depolarization. In contrast, during injection of 0.25 nA into the apical dendrite 0.6λ from the soma (right), a full dendritic Ca spike occurs, associated with bursting in the soma and more proximal dendrites. Burst envelope in the model CA1 is smaller than in the model CA3 cell, presumably because of smaller total g_{Ca} in the CA1 model. CA1 model, unlike the CA3 model, does not exhibit periodic bursting during injection of a steady current, even into the dendrites.

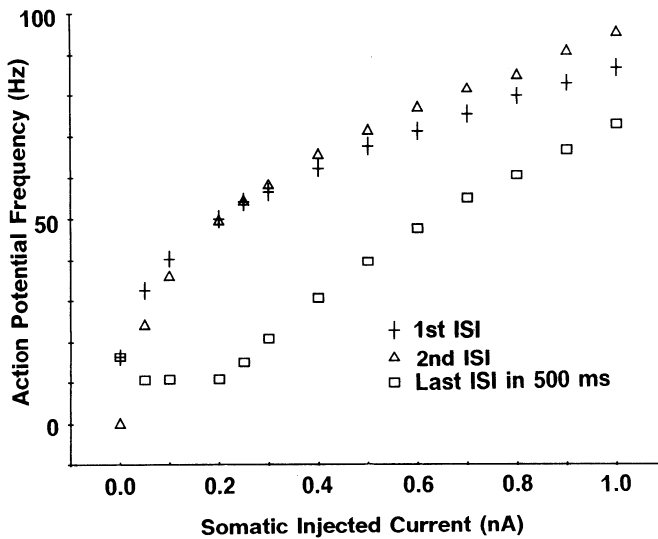


FIG. 13. *fI* curves for CA1 cell model, showing data for the 1st, 2nd, and steady-state interspike interval (ISI). There is significant adaptation between the 1st and last ISI, but, unlike most CA1 cells in the slice, not between the 1st and 2nd ISI. We attribute this discrepancy to the model's development of a dendritic depolarization that transiently tends to accelerate firing before outward currents (e.g. $g_{K(AHP)}$) slow it down.

Synchronized multiple bursts: the problem

We now turn to the issue of networks of CA3 pyramidal neurons interconnected by their recurrent excitatory synapses. This is a matter about which we have written extensively (for review see Traub and Miles 1991b; Wong et al. 1986). The essential ideas are these: 1) the density of CA3 recurrent excitatory synapses in the slice is high enough that, on average, each pyramidal cell excites many other pyramidal cells (Miles and Wong 1987a; Traub and Miles, 1991b). 2) The monosynaptic excitatory connections are powerful enough that, with probability of about $1/2$, a presynaptic burst of action potentials can elicit a postsynaptic burst (Miles and Wong 1986, 1987; Traub and Miles 1991b). 3) With these network features and with $GABA_A$ inhibition blocked, one expects that local stimulation, perhaps even to one cell, should elicit a chain reaction of rapidly spreading excitation, culminating in the synchronized firing of all of the cells—the paroxysmal depolarizing shift (PDS). Such events do occur (Miles and Wong 1983; Wong and Traub 1983) and are associated with the large synaptic excitation to each cell expected from the simultaneous firing of all of its synaptic inputs (Johnston and Brown 1981). Furthermore, one can readily reproduce this type of network behavior in great detail with a single-cell model that does not incorporate voltage-clamp data (Traub and Wong 1982; Traub et al. 1987), even in a model without a description of distinct membrane ionic currents at all (Traub and Wong 1983).

In the presence of $GABA_A$ blocking agents, however, a more complex type of network behavior often occurs, a behavior not so readily explained. In this behavior, synchronized multiple bursts occur (Hablitz 1984; Miles et al. 1984). The first burst is longer than subsequent ones. The later bursts appear at intervals of ~ 60 ms. These events occur spontaneously and can be evoked by stimulating a single cell. A critical number of cells, $\sim 1,000$, is required

for their appearance. Excitatory synaptic transmission is necessary for the generation of synchronized multiple bursts, and a transient synaptic signal appears in phase with each burst (Miles et al. 1984). We could not succeed in reproducing synchronized multiple bursts with our previous single-cell model unless rather ad hoc properties of the excitatory synapses or recurrent axons were postulated (Traub et al. 1984).

Synchronized multiple bursts represent a complex interaction between dual-action excitatory synapses and intrinsic dendritic conductances

The present single-cell model is able to generate brief bursts at ~ 15 Hz (Figs. 9 and 11) when the dendrites are excited. Furthermore, since our 1984 study, the NMDA receptor has been at least partially characterized. In particular, the conductance produced by activation of the NMDA receptor when the cell is depolarized can relax with a time constant of >100 ms (Forsythe and Westbrook 1988). Let us hypothesize that recurrent excitatory synapses between CA3 neurons involve both QUIS receptors and NMDA receptors. It appears likely that QUIS receptors occur, because 6-cyano-7-nitroquinoxaline-2,3-dione (CNQX) can abolish synchronized firing in CA3 (Chamberlin et al. 1990). Although we are not aware of direct experimental evidence for NMDA receptors at recurrent CA3 excitatory synapses, this is a plausible assumption in view of the likely occurrence of NMDA receptors at Schaffer collateral synapses (Davies and Collingridge 1989) and of the results of binding studies in the hippocampus (Monaghan and Cotman 1985).

If it is true that the recurrent CA3 synapses contain an NMDA component, then recurrent excitation could provide tonic dendritic excitation. QUIS EPSPs would not only mediate the spread of bursting throughout the population, but also depolarize the dendrites enough to unblock the NMDA-activated channels. Activation of dendritic NMDA receptors would then elicit repetitive dendritic calcium spikes, expressed at the soma as brief bursts. Short-duration EPSPs could help to maintain synchrony of these brief bursts.

Figure 14 demonstrates that these ideas are at least consistent. To generate this simulation, we constructed a network of 100 identical model pyramidal cells. Although this may be unrealistically small, the number of inputs per cell, 20, was about right for a network of 1,000 CA3 pyramidal cells. The parameter c_{QUIS} was 4 nS and a peak unitary NMDA EPSP was 3 nS. The mathematical form of these EPSPs is described in METHODS. We found it necessary to include saturation of the NMDA conductance, so that (in the present case) no cell could develop a total NMDA conductance of >187.5 nS. Without this saturation, the NMDA conductance would become excessively large owing to temporal summation of the very slowly decaying unitary events. A holding current of -0.05 nA was applied to all of the cells to suppress spontaneous firing, and a single cell was stimulated with a 0.1-nA steady current.

What develops under these conditions is a synchronized series of cellular bursts, terminated (as appropriate) by an AHP (Fig. 14). Note that the QUIS synaptic input is modu-

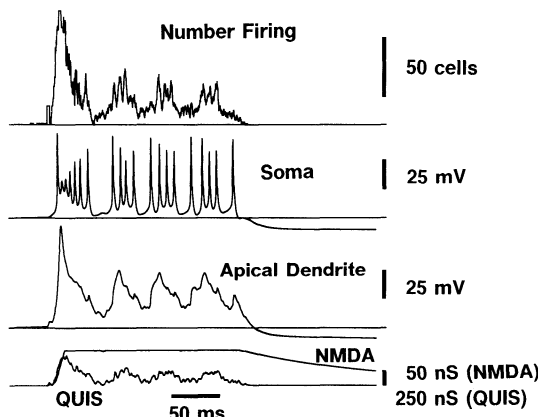


FIG. 14. Synchronized multiple bursts in a randomly connected network of 100 model CA3 neurons. Each neuron receives input from 20 others. All synapses are excitatory and contain quisqualate (QUIS, rapid time course, not voltage dependent) and NMDA (slow time course, voltage dependent) components. Synaptic excitation occurs onto compartments 3 and 15 (see the bottom of Fig. 1). Parameter ξ in the NMDA voltage-dependence was 50 mV (see text). The NMDA “virtual conductance” (that is, ignoring the voltage-dependent factor) saturates in the model. This simulation has no synaptic inhibition. A stimulus was given to one cell. There is the rapid (tens of ms) development of a synchronized population burst followed by a series of less synchronized bursts. These bursts are apparent in the soma of a particular cell (Soma), whereas, 0.6 λ apically (Apical Dendrite), slow rhythmic waves occur. These waves are partly regenerative calcium spikes, partly synaptic. Synaptic conductances plotted below for this cell are local dendritic conductances. NMDA signal plotted is the virtual conductance.

lated in phase with the total population activity. The simulation demonstrates that our hypothesis on multiple-burst generation is plausible. Nevertheless, the simulation is not perfect: the initial burst is too short (durations of ~ 200 ms often occur experimentally), and the depolarizing envelope of the somatic bursts is too small. Nor could we readily adjust the parameters so as to generate a larger number of bursts. Presumably, this simulation will become more realistic as more of the relevant parameters are determined experimentally. We note that the general phenomenon of synchronized multiple bursts in the present model does not require a “critical” choice of parameters; that is, c_{QUIS} , the unitary NMDA conductance, and the level of NMDA saturation can all be varied.

DISCUSSION

We have presented models of CA3 and CA1 pyramidal cells that incorporate, to the best of our ability, voltage-clamp data from Na, high-voltage-activated Ca, and four different K currents. The densities of channels on the soma were also constrained by experimental data. The densities of channels in the dendrites and the kinetics of intracellular calcium (in a thin submembrane shell) were treated as free parameters and were tuned so as to reproduce as wide a variety as possible of current-clamp experiments.

The model is successful at reproducing the different types of firing behavior elicited by brief current pulses or by small or large depolarizing currents injected into the soma. In particular, simulations reproduce the phenomenon of low-frequency bursting during injection of a small depolarizing current, higher-frequency repetitive firing with a large current, and a mixture in between. The model’s success

here appears to depend on the different densities of the various ionic channels in different parts of the cell membrane, an idea long advanced by Rodolfo Llinás in the context of other cells. Of particular relevance is the ability of the cell to generate large dendritic calcium spikes in a manner susceptible to blockade by local shunting of the membrane.

This model predicts that such a mode of repetitive firing, with dendritic calcium spikes, can occur during stimulation of the middle or distal dendrites (either apical or basilar). This provides a possible experimental test of the model. Nevertheless, it may not be trivial to test experimentally for the occurrence of this mode of firing, because stimulation of a dendritic compartment in the model (with its equivalent cylinder representation of each set of dendrites) corresponds to stimulation of numerous dendritic sites that may not be spatially localized in an actual cell. Application of glutamate microdrops might be one approach.

We propose that this “dendritic” mode of firing, if confirmed, is critical for the generation of synchronized afterdischarges that occur often in the presence of picrotoxin in hippocampal slices, as well as after repeated tetanic stimulation of CA3 afferent fibers (Miles and Wong 1987b). A means of tonically exciting the dendrites also appears necessary for afterdischarges. Collective activation of NMDA receptors could play this role (as in Fig. 14). Conceivably, however, a slowly inactivating, intrinsic membrane depolarizing current could serve just as well. The presumed occurrence of repetitive calcium spikes under conditions known to produce synaptic plasticity (that is, repetitive stimulation of afferent fibers) suggests an important functional role of these membrane events in learning and memory. There are, however, too many gaps in our knowledge to permit us to speculate usefully on this issue.

If, as our model suggests, a long-lasting dendritic NMDA current leads to repetitive dendritic Ca spikes during synchronized multiple bursts, then NMDA blockers such as D-2-amino-5-phosphonovaleric acid (APV) should suppress the secondary bursts while not blocking completely the initial synchronized burst. There is experimental support for this prediction in rat amygdala induced to generate multiple bursts by 4-aminopyridine (Fig. 5 of Gean et al. 1990). A similar experiment on hippocampal slices bathed in picrotoxin would help to test our model.

For comparing our simulation results with calcium-imaging data (with, e.g., intracellular FURA or Arsenazo), it is important to recall that calcium-imaging experiments “see” free calcium within the entire cell interior. In contrast, the relevant quantity in our model is χ , the calcium concentration within a small submembrane shell. One way of bridging this gap between theory and experiment is to include in the model a theoretical description of intracellular calcium movement (Ahmed and Connor 1988; Yamada et al. 1989; Zucker 1989). Such an approach, however, is computationally quite involved and involves many troubling uncertainties, including the stimulated release of calcium from intracellular organelles (Hernandez-Cruz et al. 1990).

A final issue concerns the extent to which network results obtained with our previous simpler single-cell model have general validity, that is, are dependent on details of the sin-

gle-cell model. Many simulations of networks of 100 and 1,000 neurons using the present single-cell model, and with populations of inhibitory cells that generate either GABA_A or γ -aminobutyric acid-B (GABA_B) inhibition, suggest that the basic results on population behaviors in CA3 networks, summarized in Traub and Miles (1991b), still occur. In particular, we are still able to observe low-amplitude population oscillations, in which a relatively regular population rhythm (expressed as synchronized synaptic potentials in single cells) occurs, with irregular patterns of firing in individual cells (Miles and Wong 1987; Schneiderman 1986; Schwartzkroin and Haglund 1986; Traub et al. 1989). The paper of Traub and Miles (1991a) provides some examples.

R. D. Traub acknowledges ideas stemming from earlier collaboration with Dr. R. Llinás. We thank Dr. Alan Kay for many helpful discussions on g_{Ca} and for sharing unpublished data on its inactivation kinetics. We thank Drs. C. F. Stevens and C. E. Jahr for sharing then-unpublished data on the quantitative aspects of NMDA conductance activation; Drs. W. N. Ross and N. L. Ross for sharing some unpublished data on calcium-imaging of Purkinje cells; and Dr. D. A. Turner for sharing unpublished data on the electrotonic properties of CA3 pyramidal cells. We thank Drs. J. G. R. Jefferys and A. Ives for helpful discussions.

This work was supported by IBM, the National Institutes of Health (NS-24519), the Klingenstein Foundation, and INSERM.

Address for reprint requests: R. D. Traub, IBM Research Division, IBM T. J. Watson Research Center, Yorktown Heights, NY 10598.

Received 29 November 1990, accepted in final form 28 March 1991.

REFERENCES

- ADAMS, P. R., CONSTANTI, A., BROWN, D. A., AND CLARK, R. B. Intracellular Ca²⁺ activates a fast voltage-sensitive K⁺ current in vertebrate sympathetic neurones. *Nature Lond.* 296: 746–749, 1982.
- AHMED, Z. AND CONNOR, J. A. Calcium regulation by and buffer capacity of molluscan neurons during calcium transients. *Cell Calcium* 9: 57–69, 1988.
- ALGER, B. E. AND WILLIAMSON, A. A transient calcium-dependent potassium component of the epileptiform burst after-hyperpolarization in rat hippocampus. *J. Physiol. Lond.* 399: 191–205, 1988.
- BROWN, T. H. AND JOHNSTON, D. Voltage-clamp analysis of mossy fiber synaptic input to hippocampal neurons. *J. Neurophysiol.* 50: 487–507, 1983.
- CHAMBERLIN, N. L., TRAUB, R. D., AND DINGLEDINE, R. Role of EPSPs in initiation of spontaneous synchronized burst firing in rat hippocampal neurons bathed in high potassium. *J. Neurophysiol.* 64: 1000–1008, 1990.
- DANIEL, J. W. AND MOORE, R. E. *Computation and Theory in Ordinary Differential Equations*. San Francisco, CA: Freeman, 1970.
- DAVIES, S. N. AND COLLINGRIDGE, G. L. Role of excitatory amino acid receptors in synaptic transmission in area CA1 of rat hippocampus. *Proc. R. Soc. Lond. B Biol. Sci.* 236: 373–384, 1989.
- FISHER, R. E., GRAY, R., AND JOHNSTON, D. Properties and distribution of single voltage-gated calcium channels in adult hippocampal neurons. *J. Neurophysiol.* 64: 91–104, 1990.
- FORSYTHE, I. D. AND WESTBROOK, G. L. Slow excitatory postsynaptic currents mediated by N-methyl-D aspartate receptors on cultured mouse central neurones. *J. Physiol. Lond.* 396: 515–533, 1988.
- FRENCH, C. R., SAH, P., BUCKETT, K. J., AND GAGE, P. W. A voltage-dependent persistent sodium current in mammalian hippocampal neurons. *J. Gen. Physiol.* 95: 1139–1157, 1990.
- GEAN, P.-W., CHOU, S.-M., AND CHANG, F.-C. Epileptiform activity induced by 4-aminopyridine in rat amygdala neurons: the involvement of N-methyl-D-aspartate receptors. *Eur. J. Pharmacol.* 184: 213–221, 1990.
- HABLITZ, J. J. Picrotoxin-induced epileptiform activity in the hippocampus: role of endogenous versus synaptic factors. *J. Neurophysiol.* 51: 1011–1027, 1984.
- HABLITZ, J. J. AND JOHNSTON, D. Endogenous nature of spontaneous bursting in hippocampal pyramidal neurons. *Cell. Mol. Neurobiol.* 1: 325–334, 1981.
- HALLIWELL, J. V. AND ADAMS, P. R. Voltage-clamp analysis of muscarinic excitation in hippocampal neurons. *Brain Res.* 250: 71–92, 1982.
- HERNÁNDEZ-CRUZ, A., SALA, F., AND ADAMS, P. R. Subcellular calcium transients visualized by confocal microscopy in a voltage-clamped vertebrate neuron. *Science Wash. DC* 247: 858–862, 1990.
- HOTSON, J. R. AND PRINCE, D. A. A calcium-activated hyperpolarization follows repetitive firing in hippocampal neurons. *J. Neurophysiol.* 43: 409–419, 1980.
- HOTSON, J. R., PRINCE, D. A., AND SCHWARTZKROIN, P. A. Anomalous inward rectification in hippocampal neurons. *J. Neurophysiol.* 42: 889–895, 1979.
- ISHIZUKA, N., WEBER, J., AND AMARAL, D. G. Organization of intrahippocampal projections originating from CA3 pyramidal cells in the rat. *J. Comp. Neurol.* 295: 580–623, 1990.
- JAHR, C. E. AND STEVENS, C. F. Voltage dependence of NMDA-activated macroscopic conductances predicted by single-channel kinetics. *J. Neurosci.* 10: 3178–3182, 1990.
- JOHNSTON, D. AND BROWN, T. H. Giant synaptic potential hypothesis for epileptiform activity. *Science Wash. DC* 211: 294–297, 1981.
- KAY, A. R. Inactivation kinetics of the calcium current of acutely dissociated CA1 pyramidal cells of the mature guinea pig hippocampus. *J. Physiol. Lond.* In press.
- KAY, A. R. AND WONG, R. K. S. Isolation of neurons suitable for patch-clamping from adult mammalian central nervous systems. *J. Neurosci. Methods* 16: 227–238, 1986.
- KAY, A. R. AND WONG, R. K. S. Calcium current activation kinetics in isolated pyramidal neurones of the CA1 region of the mature guinea-pig hippocampus. *J. Physiol. Lond.* 392: 603–616, 1987.
- KONNERTH, A., LUX, H.-D., AND HEINEMANN, U. Ionic properties of burst generation in hippocampal pyramidal somata ‘in vitro.’ *Exp. Brain Res. Suppl.* 14: 368–374, 1986.
- LACAILLE, J.-C., MUELLER, A. L., KUNKEL, D. D., AND SCHWARTZKROIN, P. A. Local circuit interactions between oriens/alveus interneurons and CA1 pyramidal cells in hippocampal slices: electrophysiology and morphology. *J. Neurosci.* 7: 1979–1993, 1987.
- LANCASTER, B. AND ADAMS, P. R. Calcium-dependent current generating the afterhyperpolarization of hippocampal neurons. *J. Neurophysiol.* 55: 1268–1282, 1986.
- LANCASTER, B. AND NICOLL, R. A. Properties of two calcium-activated hyperpolarizations in rat hippocampal neurones. *J. Physiol. Lond.* 389: 187–203, 1987.
- LANTHORN, T. H., STORM, J., AND ANDERSEN, P. Current-to-frequency transduction in CA1 hippocampal pyramidal cells: slow prepotentials dominate the primary range firing. *Exp. Brain Res.* 53: 431–443, 1984.
- LESTER, R. A. J., CLEMENTS, J. D., WESTBROOK, G. L., AND JAHR, C. E. Channel kinetics determine the time course of NMDA receptor-mediated synaptic currents. *Nature Lond.* 346: 565–567, 1990.
- MASUKAWA, L. M. AND PRINCE, D. A. Synaptic control of excitability in isolated dendrites of hippocampal neurons. *J. Neurosci.* 4: 217–227, 1984.
- MAYER, M. L., WESTBROOK, G. L., AND GUTHRIE, P. B. Voltage-dependent block by Mg²⁺ of NMDA responses in spinal cord neurones. *Nature Lond.* 309: 261–263, 1984.
- MILES, R. Variation in strength of inhibitory synapses in the CA3 region of guinea pig hippocampus in vitro. *J. Physiol. Lond.* 431: 659–676, 1990.
- MILES, R. AND WONG, R. K. S. Single neurones can initiate synchronized population discharge in the hippocampus. *Nature Lond.* 306: 371–373, 1983.
- MILES, R. AND WONG, R. K. S. Unitary inhibitory synaptic potentials in the guinea-pig hippocampus in vitro. *J. Physiol. Lond.* 356: 97–113, 1984.
- MILES, R. AND WONG, R. K. S. Excitatory synaptic interactions between CA3 neurones in the guinea-pig hippocampus. *J. Physiol. Lond.* 373: 397–418, 1986.
- MILES, R. AND WONG, R. K. S. Inhibitory control of local excitatory circuits in the guinea-pig hippocampus. *J. Physiol. Lond.* 388: 611–629, 1987a.
- MILES, R. AND WONG, R. K. S. Latent synaptic pathways revealed after tetanic stimulation in the hippocampus. *Nature Lond.* 329: 724–726, 1987b.
- MILES, R., WONG, R. K. S., AND TRAUB, R. D. Synchronized afterdischarges in the hippocampus: contribution of local synaptic interactions. *Neuroscience* 12: 1179–1189, 1984.
- MONAGHAN, D. T. AND COTMAN, C. W. Distribution of N-methyl-D-

- aspartate-sensitive L-[³H]glutamate-binding sites in rat brain. *J. Neurosci.* 5: 2909–2919, 1985.
- NOWAK, L., BREGESTOVSKI, P., ASCHER, P., HERBERT, A., AND PROCHIANTZ, A. Magnesium gates glutamate-activated channels in mouse central neurones. *Nature Lond.* 307: 462–465, 1984.
- NUMANN, R. E., WADMAN, W. J., AND WONG, R. K. S. Outward currents of single hippocampal cells obtained from the adult guinea-pig. *J. Physiol. Lond.* 393: 331–353, 1987.
- POOLOS, N. P., KOCSIS, J. D., PONGRACZ, F., AND SHEPHERD, G. M. Intradendritic recordings of NMDA receptor-mediated potentials in CA1 hippocampal pyramidal cells. *Soc. Neurosci. Abstr.* 16: 737, 1990.
- RALL, W. Theory of physiological properties of dendrites. *Ann. NY Acad. Sci.* 96: 1071–1092, 1962a.
- RALL, W. Electrophysiology of a dendritic neuron model. *Biophys. J.* 2: 145–167, 1962b.
- RALL, W. Cable theory for dendritic neurons. In: *Methods in Neuronal Modeling: From Synapses to Networks*, edited by C. Koch and I. Segev. Cambridge, MA: MIT Press, 1989, p. 9–62.
- REGEHR, W. G., CONNOR, J. A., AND TANK, D. W. Optical imaging of calcium accumulation in hippocampal pyramidal cells during synaptic activation. *Nature Lond.* 341: 533–536, 1989.
- SAH, P., GIBB, A. J., AND GAGE, P. W. The sodium current underlying action potentials in guinea pig hippocampal CA1 neurons. *J. Gen. Physiol.* 91: 373–398, 1988a.
- SAH, P., GIBB, A. J., AND GAGE, P. W. Potassium current activated by depolarization of dissociated neurons from adult guinea pig hippocampus. *J. Gen. Physiol.* 92: 263–278, 1988b.
- SCHNEIDERMAN, J. H. Low concentrations of penicillin reveal rhythmic, synchronous synaptic potentials in hippocampal slice. *Brain Res.* 398: 231–241, 1986.
- SCHWARTZKROIN, P. A. Further characteristics of hippocampal CA1 cells in vitro. *Brain Res.* 128: 53–68, 1977.
- SCHWARTZKROIN, P. A. Secondary range rhythmic spiking in hippocampal neurons. *Brain Res.* 149: 247–250, 1978.
- SCHWARTZKROIN, P. A. AND HAGLUND, M. M. Spontaneous rhythmic synchronous activity in epileptic human and normal monkey temporal lobe. *Epilepsia* 27: 523–533, 1986.
- SCHWARTZKROIN, P. A. AND PRINCE, D. A. Penicillin-induced epileptiform activity in the hippocampal in vitro preparation. *Ann. Neurol.* 1: 463–469, 1977.
- SPENCER, W. A. AND KANDEL, E. R. Electrophysiology of hippocampal neurons IV. Fast prepotentials. *J. Neurophysiol.* 24: 272–285, 1961.
- STORM, J. Action potential repolarization and a fast after-hyperpolarization in rat hippocampal pyramidal cells. *J. Physiol. Lond.* 385: 733–759, 1987.
- STORM, J. Temporal integration by a slowly inactivating K⁺ current in hippocampal neurons. *Nature Lond.* 336: 379–381, 1988.
- STORM, J. An after-hyperpolarization of medium duration in rat hippocampal pyramidal cells. *J. Physiol. Lond.* 409: 171–190, 1989.
- STORM, J. F. Why is the input conductance of hippocampal neurones impaled with microelectrodes so much higher than when giga-seal patch pipettes are used? *Soc. Neurosci. Abstr.* 16: 506, 1990.
- SUGIMORI, M. AND LLINÁS, R. R. Real-time imaging of calcium influx in mammalian cerebellar Purkinje cells in vitro. *Proc. Natl. Acad. Sci. USA* 87: 5084–5088, 1990.
- TANG, C.-M., DICHTER, M., AND MORAD, M. Quisqualate activates a rapidly inactivating high conductance ionic channel in hippocampal neurons. *Science Wash. DC* 243: 1474–1477, 1989.
- TRAUB, R. D. Simulation of intrinsic bursting in CA3 hippocampal neurons. *Neuroscience* 7: 1233–1242, 1982.
- TRAUB, R. D., KNOWLES, W. D., MILES, R., AND WONG, R. K. S. Synchronized afterdischarges in the hippocampus: simulation studies of the cellular mechanism. *Neuroscience* 12: 1191–1200, 1984.
- TRAUB, R. D. AND LLINÁS, R. Hippocampal pyramidal cells: significance of dendritic ionic conductances for neuronal function and epileptogenesis. *J. Neurophysiol.* 42: 476–496, 1979.
- TRAUB, R. D. AND MILES, R. Multiple modes of neuronal population activity emerge after modifying specific synapses in a model of the CA3 region of the hippocampus. *Ann. NY Acad. Sci.* 1991a.
- TRAUB, R. D. AND MILES, R. *Neuronal Networks of the Hippocampus*. New York: Cambridge Univ. Press, 1991b.
- TRAUB, R. D., MILES, R., AND WONG, R. K. S. Models of synchronized hippocampal bursts in the presence of inhibition. I. Single population events. *J. Neurophysiol.* 58: 739–751, 1987.
- TRAUB, R. D., MILES, R., AND WONG, R. K. S. Model of the origin of rhythmic population oscillations in the hippocampal slice. *Science Wash. DC* 243: 1319–1325, 1989.
- TRAUB, R. D. AND WONG, R. K. S. Cellular mechanism of neuronal synchronization in epilepsy. *Science Wash. DC* 216: 745–747, 1982.
- TRAUB, R. D. AND WONG, R. K. S. Synchronized burst discharge in disinhibited hippocampal slice. II. Model of cellular mechanism. *J. Neurophysiol.* 49: 459–471, 1983.
- TRAUB, R. D., WONG, R. K. S., AND MILES, R. A model of the CA3 hippocampal pyramidal cell based on voltage-clamp data. *Soc. Neurosci. Abstr.* 16: 1297, 1990.
- TURNER, D. A. AND SCHWARTZKROIN, P. A. Steady-state electrotonic analysis of intracellularly stained hippocampal neurons. *J. Neurophysiol.* 44: 184–199, 1980.
- TURNER, D. A. AND SCHWARTZKROIN, P. A. Electrical characteristics of dendrites and dendritic spines in intracellularly-stained CA3 and dentate neurons. *J. Neurosci.* 3: 2381–2394, 1983.
- WILLIAMSON, A. AND ALGER, B. E. Characterization of an early afterhyperpolarization after a brief train of action potentials in rat hippocampal neurons in vitro. *J. Neurophysiol.* 63: 72–81, 1990.
- WONG, R. K. S. AND PRINCE, D. A. Afterpotential generation in hippocampal pyramidal cells. *J. Neurophysiol.* 45: 86–97, 1981.
- WONG, R. K. S., PRINCE, D. A., AND BASBAUM, A. I. Intradendritic recordings from hippocampal neurons. *Proc. Natl. Acad. Sci. USA* 76: 986–990, 1979.
- WONG, R. K. S. AND TRAUB, R. D. The dendrites and somata of hippocampal pyramidal cells generate different action potential patterns. *Soc. Neurosci. Abstr.* 8: 412, 1982.
- WONG, R. K. S. AND TRAUB, R. D. Synchronized burst discharge in disinhibited hippocampal slice. I. Initiation in CA2-CA3 region. *J. Neurophysiol.* 49: 442–458, 1983.
- WONG, R. K. S., TRAUB, R. D., AND MILES, R. Cellular basis of neuronal synchrony in epilepsy. In: *Basic Mechanisms of the Epilepsies. Molecular and Cellular Approaches. Advances in Neurology*, edited by A. V. Delgado-Escueta, A. A. Ward, Jr., D. M. Woodbury, and R. J. Porter. New York: Raven, 1986, vol. 44, p. 583–592.
- YAMADA, W. M., KOCH, C., AND ADAMS, P. R. Multiple channels and calcium dynamics. In: *Methods in Neuronal Modeling*, edited by C. Koch and I. Segev. Cambridge, MA: MIT Press, 1989, p. 97–134.
- ZUCKER, R. S. Models of calcium regulation in neurons. In: *Neural Models of Plasticity*, edited by J. H. Byrne and W. O. Berry. San Diego, CA: Academic, 1989, p. 403–422.